Pristine nocturnal convective initiation: A climatology and preliminary examination of predictability

by

Sean Andrew Stelten

A thesis submitted to the graduate faculty

in partial fulfillment of the requirements for the degree of

MASTER OF SCIENCE

Major: Meteorology

Program of Study Committee:
William A. Gallus, Jr., Major Professor
Xiaoqing Wu
Raymond W. Arritt

Iowa State University

Ames, Iowa

2016

TABLE OF CONTENTS

ABSTRACT

One of the biggest forecasting challenges for Great Plains forecasters is correct prediction of convective initiation, especially when it is elevated at night. This study examines a subset of nocturnal elevated convective initiation events that occur without direct influence from surface boundaries or pre-existing convection. 287 of these events were examined over a four-month period during the summer of 2015 (May, June, July, and August). Events were first classified into one of four types based on apparent formation mechanisms and location relative to any low-level jet. A climatology of each type was performed, noting general spatial tendencies over a large Great Plains domain and initiation timing trends. Additionally, analysis of initiation elevation was performed. Five convection allowing models available during the Plains Elevated Convection At Night (PECAN) field campaign were analyzed for location and timing errors. Additionally, four versions of a 4km WRF model, each with a different planetary boundary layer (PBL) scheme were run for a few representative cases to explore predictability of these types of convective initiation.

The climatology revealed a dual-peak pattern for when initiation occurred, with one peak near 0400 UTC and another near 0700 UTC. The times that the two peaks occurred along with the prominence of the individual peaks shifted depending on the region of the domain being analyzed. Subtle patterns in location were identified, as well as elevation tendencies for the initiation. Model deficiencies tended to be more with location rather than timing for the 5 PECAN models, with the four 4km WRF models showing similar location issues plus issues with initiating convection lower than what actually happened.

CHAPTER 1. GENERAL INTRODUCTION

1.1 Background and Overview

Convective storms in the Great Plains region of the United States are extremely varied, ranging from small, short-lived air mass thunderstorms to massive Mesoscale Convective Systems (MCSs) that may be 100+km long and last hours (Maddox 1980). However, they share two major things in common. They produce rainfall essential to the agricultural economy that dominates many of the states in this area (Jirak et al. 2003), and they are often associated with hazards that can be extremely dangerous (like tornadoes, flash flooding, and lightning) to those same economies, as well as property, animals, and people. Therefore, it is extremely important that the initiation of these storms is correctly forecast by both operational forecasters and numerical models.

Daytime convective initiation is somewhat well forecast, especially when large forcing mechanisms are present like synoptic scale fronts (Jankov and Gallus 2004; Szoke et al. 2004; Wilson and Roberts 2006), although this is not always the case (Duda and Gallus 2013). With daytime heating present as well, daytime convective initiation over the Great Plains is often surface based in nature. Timing of this initiation is also often easy to predict, since an approximate forecast of initiation can be achieved through sounding analysis, looking for areas rapidly approaching their convective temperature. Additionally, surface based convection allows for use of higher density surface observations for convective forecasting, something not available when considering another form of initiation, elevated initiation.

Elevated convective initiation is simply convection that initiates at any level above the surface. While elevated convective initiation is often seen during the daytime, it is

predominantly a nighttime occurrence, just as surface-based convective initiation is possible at night, but more frequent during the day (Wilson and Roberts 2006; Trier et al. 2006). This is due to the rapid cooling of the surface after daytime heating is lost. As the surface begins to cool, the air immediately above the surface begins to stabilize, and a stable layer begins to form in the lowest level of the atmosphere. This stable layer thus forces most convection to initiate from levels other than the surface, making it elevated. At this point, some of these elevated convective initiation events may still be easily predicted, albeit only a few hours or less prior to initiation, if the events are initiated off features emanating from pre-existing convection, like gust fronts/outflow boundaries (Weckwerth and Wakimoto 1992; Moncrieff and Liu 1999). The remaining events are then particularly tricky to forecast, which are elevated and *not* directly initiated by surface features or forcing mechanisms caused by pre-existing convection, and will be the primary focus of this paper.

Elevated convection of this nature is also difficult to model. All the types of elevated convective initiation explored in this paper rely to some extent on smaller scale forcing mechanisms that usually cannot be resolved by models unless they are run at a high enough resolution and with high resolution initial conditions, which would then pose the need for increased computer resources. One type, to be explained later, relies on the correct prediction of a parent MCS, resulting in similar issues to those associated with predicting "bow and arrow" style initiation (Keene and Schumacher 2013).

Pristine elevated convective initiation, initiation occurring without direct interference by surface boundaries or pre-existing convection, is starting to become a bigger research focus, and was one of the four main objectives of the Plains Elevated Convection At Night (PECAN) field campaign. While this type of initiation may be subtle and nuanced, it

still can result in significant weather impacts, which can be seen in some of the cases studied in this paper. This thesis details a basic climatology of nocturnal elevated convective initiation events during four summer months in 2015 to reveal any temporal and spatial trends in initiation events. Additional analysis of thermodynamic profiles from several cases of nocturnal elevated convective initiation are presented to see if trends exist in the height at which initiation occurs. Next, a basic model verification of both operational and experimental convection allowing models (CAMs) available to forecasters during the PECAN field phase was performed to study the predictability of these initiation events. Finally, several simulations of the Weather Research and Forecasting (WRF) model were conducted to investigate how different PBL schemes, and thus ways of predicting the behavior of the nocturnal stable layer, affect prediction of nocturnal pristine elevated convective initiation. The eventual goal of this study is a better understanding of this difficult to predict form of convective initiation to facilitate further research into the subtle forcing mechanisms that often come into play.

1.2 Thesis Organization

This thesis follows the journal paper format. Chapter 1 includes the general introduction and organization of the thesis. Chapter 2 contains a literature review of previous studies that have focused on convective initiation in general, both daytime and nocturnal, as well as differences and difficulties that are seen in nocturnal convective initiation forecasting (both human and model) not seen in daytime convective initiation forecasting. Chapter 3 is the paper that will be submitted to Weather and Forecasting, written by primary author Sean A. Stelten and supervising author William A. Gallus, a

graduate student and professor, respectively, in the Department of Geological and Atmospheric Sciences at Iowa State University. This chapter contains the bulk of the research performed. Finally, Chapter 4 contains the general conclusions for the entire thesis. After the main chapters, references and overall acknowledgements are listed.

CHAPTER 2. LITERATURE REVIEW

Unlike nocturnal elevated convective initiation, daytime convective initiation has been studied extensively. Outside of large scale processes and dynamics like Positive Vorticity Advection (PVA) and Warm Air Advection (WAA), mesoscale forcing mechanisms like drylines, topographical forcing, and other convergence lines/zones tend to be the focus for convective initiation, although they do tend to be linked back to the overall synoptic pattern as well as linked to smaller scale processes (Doswell 1987).

Many studies have been published to attempt to better identify atmospheric trends that may lead to convective initiation. Trends in convergence lines like drylines, both locational and strength, have been studied and linked to probability of convective initiation (Wilson and Scheiber 1986; Wilson and Roberts 2006). Drylines have been extensively studied in relation to convective initiation. They have been found to be an especially favorable area for convective initiation, with enhanced areas of convergence occurring at various intervals along the dryline due to intersections with Horizontal Convective Rolls (HCRs) and other smaller convergence lines. Additionally, initiation has been found to commonly occur on or 25-30 km east of the dryline (Ziegler et al. 1997; Ziegler and Rasmussen 1998; Hane et al. 2002; Xue and Martin 2006). Gust fronts and outflow boundaries, isolated and colliding in nature, have also been well established as important focuses for convective initiation (Mahoney 1988; Weckwerth and Wakimoto 1992; Kingsmill 1995; Moncrieff and Liu 1998). Additionally, Banacos and Schultz (2005) found that while trends in Moisture Flux Convergence (MFC) had been used as a way of monitoring convective initiation for years, horizontal mass convergence (a term in the MFC equation) by itself may predict initiation as well or better than MFC. More recently, tracking of cumulus clouds and

other features using satellite technology has provided an additional tool for short range convective initiation forecasts. An algorithm to identify and track cumulous clouds that are likely to develop into rain producing storms was proposed in Mecikalski and Bedka (2006). This algorithm identified individual clouds capable of producing convective rainfall using Geostationary Operational Environmental Satellite (GOES) data and subsequently tracked the movement of those clouds as well as monitored cloud top trends. Ultimately, probability of convective initiation was determined from accumulation of those trends and correlated to trends seen during previously analyzed convective initiation events, or when the first 35 dBZ radar reflectivity was seen (Roberts and Rutledge 2003). This method was estimated to give up to a 45-60 minute lead time for convective initiation. Despite the advances in daytime convective initiation prediction, much of what has been learned cannot be easily translated to nighttime convective initiation. This is due to several of the forecasting methods relying on visible satellite observations, which are only usable during the day, as well as certain factors that lead to daytime convective initiation, like daytime heating and the effectiveness of the dryline, being absent after dark.

Since many of what would be considered typical forcing mechanisms, such as daytime heating, are absent for nocturnal convective initiation, some research has also been devoted to uncovering elevated nocturnal initiation mechanisms. While gust fronts and other surface based features discussed earlier may be considered nocturnal features, since many of them result from nocturnal convection, they are not the primary focus of this paper since their predictability is much higher than the less predictable nocturnal elevated initiation. Wavelike features, including gravity waves and bores, have been identified as possible triggers for elevated nocturnal convective initiation (Uccellini 1975; Koch and Clark 1999;

Knupp 2006). Koch and Clark (1999), however, found that in some cases a bore by itself may not provide enough lift to initiate convection and may rely on other forcing mechanisms (like a density current) to provide further lifting of the parcels. Koch and Clark (1999) also noted that convection initiated along the line of interest *without* the presence of a bore, showing that convective initiation at night is likely extremely dependent on the overall thermodynamic and kinematic conditions in the area.

Specifying further, initiation that occurs at night, elevated, and without the presence of contamination by pre-existing convection poses an extremely difficult forecasting problem, and one that has not been researched as extensively as other forms of convective initiation. The International H_2O Project (IHOP_2002) was one project that touched on this type of convective initiation. Several of the elevated cases included convective initiation as a result of frontal overrunning of the low level jet, with elevated convergence along the jet nose. These events often grew upscale into large MCSs (Wilson and Roberts 2006; Marsham et al. 2011). However, these previous studies did not address several other types of elevated, non-contaminated convection that are often seen by Great Plains forecasters, including initiation within the LLJ, linear initiation ahead of a forward moving linear system, and initiation occurring without any obvious forcing mechanism (R. Roberts, National Center for Atmospheric Research, 2015, personal communication). Likewise, many studies have been performed to identify model tendencies and points of failure for convective initiation (Weisman et al. 1997; Trier et al. 2004 and 2006), but little has been done for this subset of elevated nocturnal convective initiation.

PRISTINE NOCTURNAL CONVECTIVE INITIATION: A CLIMATOLOGY AND PRELIMINARY EXAMINATION OF PREDICTABILITY

A paper to be submitted to *Weather and Forecasting*

Sean Stelten and William A. Gallus, Jr.

3.1 Abstract

The prediction of convective initiation remains a challenge to forecasters in the Great Plains, especially for elevated events at night. This study examines a subset of nocturnal elevated convective initiation events that occur without direct influence from surface boundaries or pre-existing convection. 287 of these events were examined over a four-month period during the summer of 2015 (May, June, July, and August). Events were first classified into one of four types based on apparent formation mechanisms and location relative to any low-level jet. A climatology of each of the four types was performed, noting general spatial tendencies over a large Great Plains domain and initiation timing trends. Additionally, analysis of initiation elevation was performed. Simulations from five convection allowing models available during the Plains Elevated Convection At Night field campaign, along with four versions of a 4km WRF model were used to examine predictability of these types of convective initiation.

The climatology revealed a dual-peak pattern for initiation timing with one near 0400 UTC and another near 0700 UTC. The times and prominence of each peak shifted depending on the region of the domain being analyzed. Subtle differences in location and elevation of

the initiation for the different types were identified. Model deficiencies tended to be more with location rather than timing for the 5 PECAN models, with the four 4km WRF models showing similar location issues plus issues with initiating convection lower than what actually happened.

3.2 Introduction

In the Great Plains region of the United States, it is well known that a large portion of warm season rainfall is a result of nocturnal convection (Wallace 1975; Maddox 1980; Fritsch and Maddox 1981; Maddox 1983; Carbone et al. 2002; Parker 2008). Mesoscale Convective Systems (MCSs), usually present during the night (Maddox 1980; Velasco and Fritsch 1987; Miller and Fritsch 1991; Bentley and Mote 1998), often are associated with some nocturnal convective initiation, even if the initiation stage of many MCSs occurs prior to sunset. MCSs can pose a threat to public safety and property due to their association with high winds, flooding, and occasionally tornadoes, despite their helpful role as being a primary producer of warm season precipitation in the central United States (Maddox et al. 1979; Maddox 1980; Fritsch et al. 1986; Rochette and Moore 1996). Thus, correctly predicting the initiation of MCSs, as well as other less organized convection, is an integral part of forecasting for the Great Plains.

Unfortunately, prediction of the convective initiation (CI) that leads to nighttime convection is quite challenging. Duda and Gallus (2013) found that, while previous studies had shown that quantitative precipitation forecast skill as well as prediction of upscale evolution increased as the strength of the large-scale forcing increased (Jankov and Gallus 2004; Szoke et al. 2004), convective initiation forecast skill did not follow such trends when

modeling using a 3km Weather Research and Forecasting (WRF) model. Wilson and Roberts (2006), however, found that convective initiation tended to be better predicted in a 10km version of the Rapid Update Cycle (RUC) when the forcing mechanism was a synoptic scale front rather than a smaller scale feature like an outflow boundary. These two studies show there is much variability associated with convective initiation. The challenge becomes even greater when the initiation takes place some distance away from any synoptic forcing feature, like a front or a low pressure system. In these cases, smaller scale features with lower predictability drive initiation, including *indirect* effects of surface boundaries (for example, convection caused by overrunning of the low level jet over a surface front or boundary instead of initiation by *just* the boundary) and interactions with the Great Plains southerly low-level jet (LLJ). The LLJ, a relatively narrow stream of air with a speed maximum occurring between 500 and 1000m AGL and usually around 0600 UTC (Bonner and Peagle 1970; Mitchell et al. 1995; Song et al. 2005), has been shown to be a major factor in the initiation of MCSs, which often evolve from nocturnal convective initiation. (Wallace 1975; Rochette and Moore 1996; Laing and Fritsch 1997).

Great Plains forecasters have noted that elevated nocturnal convective initiation often tends to favor a few distinct and rather diverse modes (R. Roberts, National Center for Atmospheric Research, 2015, personal communication). These modes arise from a variety of situations, including areas of obvious strong lift at the nose of the LLJ as it crosses over a front, to regions where no forcing mechanism is obvious. Past research has described some of these types of nocturnal convective initiation. Nighttime elevated convective initiation characteristics were examined by Wilson and Roberts (2006) for cases that occurred during the International H_2O Project (IHOP) in 2002. That study found elevated initiation episodes

to be associated with convergence of winds on the meso- and synoptic-scale between 900 and 600 hPa. This would imply an active role by the LLJ. However, no definitive time based pattern was observed for these cases, meaning simple LLJ explanations, like the elevated initiation being caused by the temporal evolution of the LLJ, were not appropriate. Colman (1990) performed a 4-year climatology of elevated nocturnal CI, but only considered frontal overrunning cases, Type 1 CI. It was found that a diurnal variation of elevated convection seemed to exist, with the peak depending on the front type (closer to 1200 UTC for warm and stationary fronts, 0000 UTC for cold fronts). While these are both important findings, neither addresses the entire nocturnal elevated convective initiation spectrum noted by forecasters, as both studies focus on either surface features or convergence zones.

Identification and study of nocturnal elevated convective initiation was one of the four main objectives during the Plains Elevated Convection At Night (PECAN) field campaign that took place between June 1st and July 16th, 2015 (Geerts et al. 2016). Since extensive data collection and analysis of these events has and will continue to be performed, the present study is centered temporally over the PECAN field phase, but the full study period has been expanded to encompass 4 warm season months, May to August, 2015 to allow for a larger sample of events. A basic climatology of all nocturnal elevated convective initiation events during this period is presented to reveal any temporal and spatial trends in initiation events during these months. Additionally, thermodynamic profiles from several cases of nocturnal elevated convective initiation are analyzed to see if trends exist in the level of initiation. Finally, a basic model verification of both operational and experimental convection allowing models (CAMs) available to forecasters during the PECAN field phase was performed to study the predictability of these initiation events. The goal of the present study is to identify

basic characteristics and prediction deficiencies of nocturnal elevated convective initiation to facilitate further investigation into physical causes of it, and ultimately better forecasting capabilities for this relatively hard to predict weather phenomenon.

3.3 Data and Methodology

3.3.1 Classification of CI events

This study examines pristine elevated nocturnal convective initiation (hereafter, PNCI) cases during May, June, July, and August of 2015. Several dates were omitted from analysis due to lack of either level 2 NWS WSR-88D radar data (28 May) or lack of available RAP analyses (20 June and 1-8 August). In the present study, PNCI is defined as initiation of convection occurring between 0000 UTC and 1200 UTC, not directly influenced by a surface feature (in other words, the initiation must be elevated), and not a result of interference from pre-existing convection (outflow boundaries, for example).

For general classification, events were preliminarily chosen by examining mosaic radar images obtained from the UCAR Meteorological Case Study Selection Kit Image Archive (www2.mmm.ucar.edu/imagearchive/). These half-hourly mosaic images were examined for convective initiation within the domain and within the 0000 UTC – 1200 UTC period. If an event seemed to be PNCI, then the date, approximate time, and the NEXRAD site(s) involved in the event were noted. After preliminary identification was complete, archived Level 2 radar data from the NWS WSR-88D radars active in each case was obtained from the National Centers for Environmental Information (NCEI) Hierarchical Data Storage System (HDSS) Access System (NCEI HAS). The 28 sites included in this study, as well as the overall domain, can be seen in Fig (1). The overall domain was split into three subdomains, “Upper

Plains", "PECAN", and "Texas". These were chosen to allow for better comparison and linkage to the PECAN project, so the PECAN subdomain roughly mirrors the effective study domain used during the actual project. The Upper Plains subdomain then encompasses everything north of the PECAN subdomain, while the Texas subdomain is everything south of the PECAN subdomain. Level 2 data were analyzed using the Gibson-Ridge Analyst Version 2 (GR2Analyst 2.0) radar software, which allows for in depth analysis of the full resolution Level 2 data, including coordinate and beam height readouts for each resolution cell.

Each preliminary event was examined to determine if it was truly PNCI, based on the criteria stated above. A convective initiation event was said to have occurred if at least one cell reached 35dBZ over a 4 km^2 area, as in Roberts and Rutledge (2003) and modified from 40dBZ over 4km^2 as in Wilson and Roberts (2006). 35dBZ was used to stay consistent with initiation criteria used during the PECAN field campaign. Then, the location of each event was determined through the coordinate readout on the GR2Analyst software. Since many events consisted of multiple cells in varying orientations a centroid method, where the general centroid of the area encompassed by the initiation event was determined, was employed to obtain one defining initiation location. Initiation time was also recorded, and defined as the first time a cell in the event reached the 35dBZ over 4 km^2 threshold.

Following classification as PNCI, each event was further classified into one of the four types of PNCI. The first (Type 1 CI) includes PNCI caused by the LLJ overrunning a surface boundary or front, with the PNCI occurring on the cold (usually north) side of the front (Fig. 2). Note the core of the LLJ (Fig. 2a) crossing and nearly perpendicular to the warm front (Fig. 2b) in this case. This mode is very similar to the Type 1 Mesoscale Convective Complex

(MCC) described in Maddox (1980), and the isentropic forcing mechanism driving this mode is further discussed in Trier (2003). The second (Type 2 CI) includes CI occurring somewhere within the LLJ itself, but not in conjunction with a surface or elevated front or boundary (Fig. 3). Note the line of storms forming along the right side of the LLJ (Fig. 3a), well ahead of the cold front to the northwest (Fig. 3b). The third type (Type 3 CI) occurs in a semi-linear orientation ahead of and at least quasi-perpendicular to the leading edge of a forward propagating MCS. Type 3 can also be referred to as "T initiation", due to this initiation type's resemblance to the letter T (Fig. 4). This could be thought of as a "flipped" version of the "bow and arrow" style initiation discussed in Keene and Schumacher (2013), however "T initiation" occurs *ahead* of the MCS and its gust front/cold pool. Finally, the fourth type (Type 4 CI) includes PNCI occurring without any definitive mesoscale cause and outside of the LLJ. The Type 4 case in Fig. (5) occurs ahead of the MCS, like a Type 3 case, but with no preferred orientation and without LLJ influence, thus it was considered Type 4. It is important to note that while Type 4 initiation was here being described as occurring without any definitive *mesoscale* cause, this does not mean other synoptic scale factors, such as the influence of a shortwave, are not in play.

To distinguish each event type, several criteria were considered. First, if an event was at least quasi-linear in orientation, within 45° of being perpendicular to a pre-existing linear system, and downstream of that system and its associated outflows, it was immediately classified as Type 3 CI. Next, 850mb winds were plotted to represent LLJ location and orientation. While some in-situ lower troposphere wind data were available for several days during the PECAN field campaign (June 1st – July 16th) via periodic rawinsonde launches at fixed and mobile sites, these data were not collected over a large enough area, at a fine

enough spatial resolution, and over a long enough period (45 days for PECAN vs 120 days needed for the present study) to be a viable data source for determining the strength, position, and orientation of the low level jet. Thus, 13km RAP analyses obtained from the NOAA National Operational Model Archive & Distribution System (NOMADS) were used as a proxy for in-situ wind measurements similar to the use of RUC analysis in Thompson et al. (2003), Schumacher and Johnson (2009), Coniglio et al. (2010), and Snively and Gallus (2014). Since strength, horizontal location, and horizontal orientation of the low level jet was considered during analysis, isotachs and wind barbs were plotted from the original constant pressure-level RAP output at 850mb using the NCAR Command Language (NCL). A LLJ was considered to have occurred during a CI event if the core of the jet reached a minimum of 12 ms^{-1}, similar to magnitudes defining Bonner I Criteria (Bonner 1968). If it was, then the CI events in question were categorized as either Type 1 or Type 2. If there was no LLJ present near the CI and no surface boundary was present, the event was classified as Type 4. Finally, 3 hourly surface maps from the Weather Prediction Center (WPC) were examined to determine if a frontal feature was also present in conjunction with the LLJ induced CI. If one was present and clearly played a role in triggering initiation, then the events were classified as Type 1, while the rest of the LLJ induced CI events were classified as Type 2. Type 2 CI events were further classified based on their location relative to the core of their associated LLJ, with sub-classifications being nose, left, middle, right, and tail (Fig. 6).

After all PNCI events had been classified according to type, Most Unstable CAPE (MUCAPE) and Mixed Layer CAPE (MLCAPE) near the CI event were analyzed to determine if there was a preferred height at which each type of elevated CI occurred and if one type of

CI tended to be more elevated than the others. Hourly SPC mesoscale analysis MUCAPE and MLCAPE plots were retrieved from the Daily Archive Directory (http://www.spc.noaa.gov/exper/ma_archive/images_s4/). Since MLCAPE in the SPC mesoanalysis is calculated using the lowest 100mb layer of the atmosphere, if a CI event exhibited more MUCAPE than MLCAPE it was assumed that the CAPE depicted by the MUCAPE plots was more elevated in nature, and that the convective initiation event was also elevated. Lifted Parcel Level (LPL), the height of the most unstable parcel, was also used to examine any variations among the PNCI types. However, the level at which the most unstable parcel resides may not be the level at which convection initiates, due to effects of Convective Inhibition (CIN). So, to further pinpoint elevation trends among the CI types, 15 cases from each type were randomly selected for further elevation analysis. As with the previous classification technique, the 15 selected Type 2 CI events were further separated into sub-groups based on their relative location to the LLJ.

CI elevation in the 60 selected cases was determined using a Skew-T based method. Hourly RAP soundings from 00 UTC to 12 UTC were plotted at the initiation location of each selected event using NCL. RAP analyses were used again for reasons similar to those stated previously. The soundings were then hand analyzed to determine magnitudes of CAPE and CIN using the basic parcel method. In this analysis, CIN was used as the predominant factor to determine at what level initiation was most likely to be happening. The pressure level that produced the least amount of CIN (while still producing more than negligible amounts of CAPE) using the parcel method was deemed the level at which convective initiation was occurring. An alternative method for determining initiation elevation was consideration of

Skew-Ts over time. If over time any one level became increasingly saturated, thus reducing CIN, this was considered a good indication that initiation was occurring at that level.

3.3.2 Model Analysis

Two approaches to model verification and analysis were used in this study. The first involved verification of five high resolution models available during the PECAN field campaign. These included the 4km WRF run by Colorado State University (CSU WRF) (http://schumacher.atmos.colostate.edu/weather/csuwrf_info.php), the Model for Prediction Across Scales (MPAS) (http://mpas-dev.github.io/), the National Severe Storms Laboratory WRF (NSSL WRF) (http://wrf.nssl.noaa.gov/newsite/index.php?about), WRF simulations performed by the Multi-scale data Assimilation and Predictability Laboratory group (WRF-MAP) (http://weather.ou.edu/~map/), and the NCEP HRRRv1 http://ruc.noaa.gov/hrrr/). Since many of these models were run regularly only during the PECAN field project, this approach to model verification was restricted to only the period during the PECAN campaign, June 1st – July 16th. Additionally, output for several of the models was archived with limited domains that encompassed mainly an area slightly larger than the original PECAN study area (Fig. 7); thus, this verification will be restricted to that domain. An important thing to note is that during the summer of 2015, the HRRRv1 experienced an issue with over-mixing of the boundary layer, thus creating a deeper and drier PBL in cases with warm 2m temperatures and dry 2m dew points, which ultimately over initiated convection during the study period (C. Alexander, NOAA/ESRL, 2015, personal communication). However, since the primary goal of this model verification was to identify the skill of forecasting tools used during PECAN, the HRRRv1 was sill included in the

verification since the over-mixing issue was not made aware to the entire forecasting team until nearly the end of the project.

Model CI initiation location and time were determined in the same way that observed CI initiation location and time were determined, by using a centroid method. Absolute error for time was calculated for each event, as well as a mean absolute distance error based on the distance of the centroid of the modeled CI event from the centroid of the observed CI event. A 90% and 95% significance level T test was performed to see if there was any significant difference in performance between each model and the overall performance of the models between types. Hit rate, false alarm rate, and threat score for each PECAN model were also calculated for each model as well as the entire group of models. For false alarm rate and threat score, a false alarm was considered to have occurred if the models produced convection that adhered to the definition of PNCI used throughout this paper. To determine if a surface boundary was in play, and thus if the falsely predicted convection was elevated, 2m temperature and wind field plots were analyzed for evidence of fronts or outflow boundaries. Additionally, WPC surface maps were used as supplements for identification of fronts, since many of the archived PECAN model temperature and winds plots suffered from sparse contours and low temporal resolution.

The second approach to model verification involved modeling a subset group of CI events to study possible failure modes in the models, which may explain why they did not handle the CI event well. This approach focused mainly on elevation differences between modeled and observed CI events, and what role PBL schemes have in these differences. Four cases were selected, one from each CI type, with criteria for selection being a large spatial area (>5000km^2) and high density (less than 20km between each individual cell) to allow

for better sounding analysis. The four cases were 24 June in eastern Nebraska and western Iowa (Type 1, Fig. 2c-f), 6 July in eastern Nebraska (Type 2, Fig. 3c-f), 22 June in southern Minnesota and northern Iowa (Type 3, Fig. 4), and 26 June in eastern Missouri (Type 4, Fig. 5). Each run used version 3.6.1 of the WRF-ARW model using 4km horizontal grid spacing. 50 vertical levels on terrain-following hydrostatic pressure coordinates were used. The domain for each model spanned 1200km by 1200km and was centered on the initiation location of the observed CI. Initial and lateral boundary conditions were provided every 6 hours from 12km NAM analysis data. Runs began at 12 UTC the day of the nocturnal initiation event, to capture the diurnal evolution of the boundary layer. WRF runs for each of the four cases were conducted using each of four PBL schemes. These schemes included two local mixing schemes, the Mellor-Yamada-Nakanishi-Niino Level 2.5 scheme (MYNN) (Nakanishi and Niino, 2009) and the Quasi-Normal Scale Elimination scheme (QNSE) (Sukoriansky et al. 2005), as well as two non-local schemes, the Yonsei University scheme (YSU) (Hong et al. 2006) and the Asymmetric Convective Model V2 scheme (ACM2) (Pleim 2007). It is important to note that the ACM2 is actually a hybrid local/non-local scheme, employing both local and non-local upward mixing and local downward mixing. Table (1) shows the remainder of the physics parameterizations used in each run.

Simulated radar reflectivity for the lowest level of the model were plotted using the wrf_user_getvar function in NCL. This function calculates reflectivity using intercept parameters for rain, snow, and graupel consistent with Reisner et al. (1998). Each plot was examined in similar fashion to the earlier initiation analysis methods, with an initiation location and time being determined for each CI event in each version of the model, and a few cases being noted where the CI event failed to occur at all. NCL was then used to create

sounding plots at both the location of the CI event in the model as well as the location of the observed CI event. If a model did not produce the CI event at all, soundings were instead plotted relative to other major areas of observed convection that *were* present in the model. If the model failed to produce any convection at all, only soundings at the observed location were plotted. These modeled soundings were then compared to the observed RAP soundings in a similar fashion.

3.4 Results and analysis

3.4.1 Climatology analysis

A general climatology for May, June, July, and August 2015 was performed for all 287 cases. Fig. (8a) shows the distribution of pristine CI events with respect to each pristine CI type. Over the 4-month period, Type 2 CI was the most common, with 153 occurrences, followed by Type 1 CI (60), Type 4 CI (46), and Type 3 CI (28). Splitting each type by month (Fig. 8b) reveals similar distributions with respect to each month, with Type 2 CI being the most common pristine CI type for all months, followed by Type 1, Type 4, and then Type 3. Type 3 and 4 were most common in June, while Type 1 was most common in July. Type 2 was also very common in July; however, it occurred most often in May. An important note to keep in mind is the fact that part of the reason August has so few cases was due to the lack of 1hr RAP analyses from 1-8 August.

Fig. (9a) shows all pristine CI cases with respect to the time that they occurred overnight. A clear peak in pristine CI activity can be seen during the 0400 UTC to 0500 UTC hour, with two smaller and less prominent peaks occurring between 0700 UTC and 0800 UTC as well as between 1000 UTC and 1100 UTC. Pristine CI times were split based on each

event's subdomain. PECAN events display a much stronger twin-peak signal at 0400 UTC – 0500 UTC and 0700 UTC - 0800 UTC (Fig. 9c) than seen in the overall domain. The Upper Plains and Texas subdomains also exhibit dual peak shape (Fig. 9b and 9d, respectively), however the time where the second peak occurs differs from each other as well as the PECAN subdomain, with Upper Plains occurring earlier at 0600 UTC – 0700 UTC and Texas occurring later at 0800 UTC – 0900 UTC with a third peak at 1000 UTC – 1100 UTC. All three subdomains show an initial peak between 0300 UTC and 0500 UTC, with Texas being slightly earlier (0300 UTC – 0400 UTC instead of 0400 UTC – 0500 UTC).

Because the double peak structure in PNCI seemed unusual, further analysis was performed to look at the timing of each individual type of CI to see if any one pristine CI type contributes to the different peaks. For the whole domain, each CI type has at least a subtle peak between 0300 UTC and 0500 UTC, corresponding with the major peak in the overall time analysis (Fig. 10a). The only exception was Type 1, which has a small peak at 0200 UTC – 0300 UTC and remains relatively constant through 0600 UTC. Since all four types have a peak at or near 0400 UTC, this implies that the peak in overall pristine CI activity at this time was *not* driven by any one type, which is especially interesting since only two of the four pristine CI types rely on LLJ activity. Since LLJ strengthening typically happens during the first half of the night (0000 UTC – 0600 UTC), one could say that the strengthening of the LLJ may be a trigger for pristine CI *if* the LLJ reliant types (Type 1 and Type 2) were the only types to exhibit this 0400 UTC peak, which was not the case. The second, minor peak at 0700 UTC – 0800 UTC seen in the overall frequency graph does appear to exist in all four types as well, but not as clearly as the first peak. In fact, Type 2 has a relative minimum at 0700 UTC – 0800 UTC with peaks both an hour earlier and an hour later. Overall, Type 3 and Type 4 CI

are relatively constant from 0500 UC to 0900 UTC, with extremely slight peaks around the 0700 UTC hour. Since the second maximum seems to be driven by the fluctuating LLJ driven pristine CI types, perhaps LLJ characteristics (its movement, strength fluctuation, etc.) are causing this second spike.

The Upper Plains subdomain shows a dual-peak pattern like the one exhibited by the overall Upper Plains frequency plot in each of the four pristine CI types, with each peak separated by about 2-3 hours (Fig. 10b). However, these peaks were offset from each other, with Type 4 occurring earlier in the night (peaks at 0100 UTC – 0200 UTC and 0400 UTC – 0500 UTC), followed by Type 1 (peaks at 0200 UTC – 0300 UTC and 0500 UTC – 0600 UTC), then Type 3 (peaks at 0300 UTC – 0400 UTC and 0600 UTC – 0700 UTC), and finally Type 2 (peaks at 0400 UTC – 0500 UTC and 0600 UTC – 0700 UTC). This staggered behavior seems to follow what would be logical when thinking about what drives each type of pristine CI and how the LLJ behaves over time. Since the main criteria for Type 3 was that initiation happens in conjunction with a pre-existing linear system, a later occurrence for a maximum makes sense because the system each Type 3 event was associated with needs to be fully formed for Type 3 initiation to take place. During the summer of 2015, most linear systems that Type 3 events occurred with formed due to upscale growth of supercells as the boundary layer decoupled and the storms became elevated. The change of mode from supercell to linear system takes several hours to accomplish, thus pushing most of the Type 3 CI later into the night. The twin peaks in Type 2 CI are centered around 0500 UTC – 0600 UTC, near when the LLJ typically was at peak strength. While there was a local minimum at 0500 UTC – 0600 UTC in the Upper Plains subdomain, which is still unexplained, the fact that the two peaks are centered over this time suggests that they are likely caused by the strengthening

and peaking of the LLJ. Meanwhile, both peaks for Type 1 CI occur about 1-2 hours earlier than the Type 2 CI peaks. A possible explanation for this could be the presence of a front/boundary in Type 1 CI events, which provides an extra forcing mechanism, thus causing initiation to happen earlier in the strengthening process of the LLJ. As for Type 4, in this subdomain at least, perhaps the shift toward earlier times for the two peaks was due to an increase reliance on the waning instability caused by daytime heating for initiation rather than more nocturnal effects.

Like the Upper Plains subdomain, the PECAN subdomain also exhibits two peaks among all 4 pristine CI types (Fig. 10c). However, the peaks occurred relatively coincident with each other, around 0300 UTC – 0500 UTC and 0700 UTC – 0900 UTC. This means that there was no one CI type contributing to one of the peaks (the early peak cannot be attributed to *just* Type 2, for example), and since they are all occurring at roughly the same time at night, LLJ development and behavior cannot necessarily be used to explain the occurrence of these peaks, since the same peaks are present in CI types that do not rely on the LLJ.

The Texas subdomain was a bit chaotic, mainly due to the small sample size for that area, which was partially caused by tropical storm Bill affecting the area during June which prevented pristine CI for several days (Fig. 10d). However, as with the PECAN subdomain, evidence of the early peak can be seen in all four pristine CI types between 0300 UTC and 0500 UTC. Evidence of the much later second peak, between 0800 UTC and 1100 UTC, appears in mainly the Type 2 CI, suggesting that at least in the southern portions of the overall domain, Type 2 tends to dominate later in the night while all four types occur equally earlier on.

Overall, the dual peak nature seen during the summer of 2015 is especially interesting. While this may suggest 2015 was not a representative year, two other unpublished studies, one completed at the end of 2015 (D. Reif, University of Oklahoma, 2015, personal communication) and one completed in 2006 (M. Dux, NWS, 2016, personal communication), performed similar analyses for general nocturnal elevated convective initiation and found similar twin peak structures. However, both studies were much longer climatologies, looking at 5+ years' worth of data rather than one summer, indicating that the results found in this study may be typical.

0-100 hPa Mixed Layer CAPE (MLCAPE; Fig. 11a) and Most Unstable CAPE (MUCAPE; Fig. 11b) values were analyzed for each pristine CI case. Events have been separated into each of the four types, showing the percentage of each PNCI type associated with no cape, low cape (0 - 1000 Jkg^{-1}), moderate cape (1000 – 2000 Jkg^{-1}), and high cape (greater than 2000 Jkg^{-1}). The CAPE values and ranges for the four categories were used in order to reflect the contour spacing of the MLCAPE and MUCAPE mesoanalysis plots that were analyzed, which tends to be 500 – 1000 Jkg^{-1} per contour, and to allow for a simple, unified method of analyzing the two different CAPE plots. Since MLCAPE is calculated using the lowest 100 hPa layer of the atmosphere, if any one type of pristine CI shows a higher frequency of being associated with low MLCAPE values and higher MUCAPE values than other types (thus meaning the highest CAPE values are occurring somewhere other than the lowest 100 hPa of the atmosphere), an assumption can be made stating that pristine CI type likely occurs *more* elevated than the others. Indeed, "no cape" events are much more common for MLCAPE than they are for MUCAPE for Types 1, 2, and 4, with "no cape" being the most common MLCAPE designation for Type 2 and 4 and a close second for Type 1. Meanwhile,

the most common MLCAPE *and* MUCAPE value for Type 3 was "moderate CAPE", suggesting that the cape associated with Type 3 events was less elevated (still elevated nonetheless, shown by the disappearance of "no CAPE" events when moving from MLCAPE to MUCAPE). With Types 1, 2, and 4 tending to exhibit more MUCAPE than MLCAPE when compared to Type 3, this infers that Type 3 may be less elevated than the other types.

While examining mesoanalysis plots of MLCAPE and MUCAPE can give a general idea of how elevated each type of CI tends to be, one of the big issues with using this approach is the fact that it cannot provide actual elevations of the pristine CI events. MUCAPE plots provided by the Storm Prediction Center's Hourly Mesoanalysis are plotted concurrently with Lifted Parcel Level (LPL), or the level at which the most unstable parcel is lifted from, but a problem exists in determining elevation height since initiation may not always be taking place at the height of the most unstable parcel. Even though a certain level may provide the most amount of elevated CAPE, that same level could also be associated with higher values of CIN, thus possibly preventing initiation from occurring. Meanwhile, another level of the atmosphere with *less* CAPE could have significantly less CIN, thus allowing convection to initiate. Thus, to reduce these problems, 15 cases from each pristine CI type were randomly selected to undergo further analysis using RAP analysis soundings to identify what level each initiation event was occurring. Averages and standard deviations for the 15 cases sampled were calculated. The average height overall at which the 60 total CI events occurred was 2540m AGL, with a standard deviation of 780m. When separating the 60 cases into Types 1 – 4, Type 4 tended to be the least elevated, with an average initiation point 2240m AGL, followed by Type 1 at 2430m AGL, Type 2 at 2740m AGL, and Type 3 at 2770m AGL. This was opposite of what the MLCAPE and MUCAPE analysis found, which suggested

that Type 3 may be the *least* elevated type of CI. Not only does sounding analysis suggest a problem with using the CAPE analysis to estimate initiation elevation, it also shows that perhaps Type 3 CI was especially sensitive to the amount of CIN present, or any other number of factors, present at the level of initiation, since most of the MUCAPE in Type 3 events tended to be less elevated. Sounding analysis of Type 3 events showing *higher* elevations suggest that this type was occurring at levels not coincident with the most unstable parcel. Standard deviations were also calculated for each pristine CI type. Of particular interest was the standard deviation for Type 2 which was 820m, larger than the other three types. This could be explained by considering the subgroups of Type 2 CI based off the location that the event occurred relative to its associated jet. Perhaps different locations relative to the jet prefer different elevations. While most of the locational subgroups are fairly similar, the "middle" subgroup clearly prefers more elevated initiation, with most cases occurring above 3000m AGL. Interestingly, this means the "middle" cases are also occurring *above* their associated jet instead of within. A representative example of this occurring can be seen in Fig. (12).

Finally, a location based analysis was completed for all pristine CI events. The primary goal of this analysis was to see if there was any preferential geographical location for any of the four pristine CI types. Fig. (13) shows locations of all pristine CI events, Fig. (14) shows locations of each CI event based on type, and Fig. (15) shows locations separated by month. Examining each of the plots, a few subtle patterns can be noted. First, there appears to be a preference for Type 4 to occur in the northern parts of the domain. A similar pattern appears for Type 1, although its signal was not as strong. Meanwhile, there appears to be a slight minimum in occurrences in the central part of the domain for Type 3, while

Type 2 occurs nearly uniformly across the domain. Separating the events by month does not reveal quite as many meaningful patterns. Overall, pristine CI events were fairly evenly distributed over the domain for each month, except for a slight minimum in the extreme northern portions of the study domain in August. While June appears to have a minimum in the southern portion, it is important to remember that the southern portion of the domain was affected by tropical storm Bill for several days, which prevented true pristine CI from occurring. Thus, such a reduction in June would not be likely if the climatology spanned more years. Finally, considering all pristine CI events (Fig. 13) there was a major clustering of events over the Nebraska/Kansas border, perhaps due to this being a typical location of the LLJ, a driving factor behind Type 1 and 2 CI.

3.4.2 Analysis of High Resolution Models Available During PECAN

High resolution models available during the PECAN field campaign included the CSU WRF, NSSL WRF, MPAS, WRF-MAP, and NCEP HRRRv1. Simulated radar output was examined for each model for each case that fell within the archived model domain. There were 99 times out of a total of 219 (60 events across 5 models, excluding any events that occurred outside the model's domain or that did not have archived plots available) when a model did not capture the CI event at all, with all the models achieving a combined hit rate of 55%, false alarm rate of 57%, and threat score of 32%. Individual model hit rates were between 39% and 64%, false alarm rates were between 49% and 65%, and threat scores were between 23% and 38% (Table 2). Of particular interest is that Type 2 CI tended to be the only type where *all* the models on occasion failed to produce the event (Table 3 and 4). Additionally, some models were not available for certain events, either due to the event

occurring outside of one of the smaller archived domains or because the model did not run on that date. The remaining cases were first analyzed based on time of occurrence. Absolute error for initiation time was calculated, with negative numbers meaning the model initiated convection earlier than what was observed, positive numbers indicating the model initiated convection later than what was observed, and 0 indicating correct time of initiation (Fig. 16). Overall, the 5 models analyzed handled timing of convective initiation rather well, exhibiting a mostly bell shaped curve when looking at all the models combined (Fig. 16a), however there was a bit of a skew toward later initiation. Examining each model separately shows mostly similar results, except that the NCEP HRRRv1 appears to favor initiating events earlier than observed (Fig. 16e) while the WRF-MAP (Fig. 16d) and CSU WRF (Fig. 16f) are skewed toward later initiation than observed. However, it should be noted that examining each model specifically yields small sample sizes, so these trends could be noise issues in the data.

Next, each model's simulated radar output was analyzed based off location of the initiation event. Locations of initiation events in the models were determined in the same way that locations of the observed pristine CI events were determined, by using a centroid approach. Once the locations of the centroids were determined, distance from the observed CI centroid was measured. Comparing the overall distance errors for each of the five high resolution models, visually the NSSL WRF and MPAS appeared to perform the best, with average distance errors of 77km and 87km, respectively (Fig. 17a). Meanwhile, the WRF-MAP, NCEP HRRRv1, and CSU WRF appeared to perform the worst, with an average distance error near 105km for all three. However, performing a T test between each of the models, at both 90% and 95% significance levels, only the NSSL WRF and the CSU WRF showed a

significant difference in distance errors, and only on the 90% significance level. Analysis of how well the models performed for each type shows, at least by appearance, that Type 4 was the worst predicted PNCI type, while Type 3 was the best predicted, in terms of location (Fig. 17b). The Type 4 result was likely due to the very subtle mechanisms that lead to this type of CI not being resolved correctly by the models. Meanwhile, Type 3 seeming to be the best predicted shows that, since Type 3 is heavily reliant on the location of its parent linear system, perhaps the models performed extremely well when predicting this system, and prediction of the location of the Type 3 PNCI is relatively simple once the parent system is established. The 5 models performed relatively the same for the two LLJ driven PNCI types, which makes sense since both are influenced by the same forcing mechanism. They did, however, appear to perform worse than the Type 3 simulated events, which do not depend on a larger scale, and often better predicted (Jankov and Gallus 2004; Szoke et al. 2004), forcing mechanism. Although, another explanation for Type 3 appearing to perform the best and Type 4 appearing to perform the worst could be simply the small sample size of each of these types, with only 7 Type 3 events and 6 Type 4 events occurring within the high resolution model domain and time period. However, like with the comparison between each model's performance, a T test was performed to compare the difference between each CI type. On both 90% and 95% significance levels, no significant difference was found between any of the four types.

3.4.3 Analysis of WRF simulated CI events

Sixteen total WRF-ARW simulations were run for four pristine CI events that occurred during the study period. Four runs per CI event were completed to analyze the effect that

variations in the boundary layer scheme used had on characteristics of the CI events (Fig. 18 – 21).

a. 24 June – Type 1

The Type 1 CI event that occurred on 24 June was a classic Type 1 frontal overrunning event. A warm front was draped west to east across northern Kansas, moving slowly northward overnight (Fig. 2b) while a rather strong LLJ, analyzed in the RAP analyses as exceeding 30 ms^{-1} was oriented SW to NE across western and central Kansas, crossing the warm front just south of the KS/NE border (Fig. 2a). This initiated convection well north of the warm front over far eastern Nebraska and into western and central IA. Initially storms were organized into several parallel lines stretching NW to SE, but quickly consolidated into a very disorganized MCS (Fig. 2c-f).

Analysis of simulated radar output of each model run reveals that the ACM2 PBL run did not produce the Type 1 CI event at all (Fig 18j-l). One possibility for this complete failure of the model was the use of the Pleim-Xiu land surface scheme for this particular run. While the other three runs used the Noah Land Surface Model as the land surface scheme, runs using the ACM2 PBL scheme were run with the Pleim-Xiu since the Pleim-Xiu surface layer scheme (recommended for use with the ACM2 PBL scheme) has only been tested for use with the Pleim-Xiu land surface scheme. So, the other three versions of the 24 June WRF-ARW model were re-run using the Pleim-Xiu land surface scheme, to see if this was the point of failure in the original ACM2 run. Very little change in simulated radar output was observed, meaning the failure point was likely in the ACM2 itself rather than the different land surface scheme. Besides this failure, the other three runs predicted the event remarkably well,

despite being slightly further west and organizing in one line instead of several parallel lines (Fig. 18a-i). All three then proceeded to develop into the weakly organized MCS seen in observations.

Modeled atmospheric profiles were taken from the centroid of CI initiation in the model at the time of initiation, similar to what was done using RAP analysis for the observed CI. In the case of the ACM2, since no pristine CI formed the sounding was simply taken from the same location as the RAP sounding used for the observed CI. One striking difference that all the models had when compared to the RAP analyses was that the level at which initiation occurred was lower in the models than it was in the RAP analysis. The level at or just above 700 hPa became increasingly saturated over time (a good indicator of convective initiation at that level) in the RAP analyses, while this occurs at about 800 to 750 hPa in the WRF models. Despite this, three of the four models obviously still produced convection. One difference that the ACM2 model exhibited that the other models did not was a slightly stronger inversion in the approximately 100 hPa layer just above the level that was becoming saturated, possibly inhibiting convection.

b. 6 July – Type 2

The Type 2 CI event that took place on 6 July fell in the "right" subgroup of the Type 2 CI events. Convection initiated in an almost perfectly straight line just SW of Omaha, NE, stretching SSW to NNE. Over time, the line grew longer, remained linear, and seemed to rotate about a vertical axis positioned over Omaha (Fig 3c-f). By 0500 UTC the linear structure began to break down, with significantly more initiation occurring between the line and the approaching MCS to the NW. This event was accompanied by another strong LLJ

(Fig. 3a), although during this Type 2 event the LLJ was in its strengthening phase, with winds reaching 25m/s over south central and eastern Nebraska toward the end of the event, as the South Dakota MCS began to overtake it.

Fig. (19) shows the simulated reflectivity for each of the four models run for this pristine CI event. None of the four captured this event at all. Surprisingly, all four models were remarkably consistent with the rest of the convection that occurred that night, including the scattered convection in NE Oklahoma and the well-organized MCS moving through southern South Dakota. In regards to the soundings produced by each model, a common theme seen among all four model runs was for the models to generally be too dry above 850 hPa. Additionally, all of them showed signs of developing at least a subtle inversion at or just above 850 hPa that was not present in the sounding produced from the RAP analysis.

c. 22 June – Type 3

The Type 3 CI event that occurred on 22 June was a very distinct example of the type, with the "T" formation quite clear. It was also one of the largest Type 3 events to occur during this study period and should therefore lend itself to be modeled well. The event began as 2-3 clusters of thunderstorms in northern South Dakota and southern North Dakota. These clusters eventually merged into a poorly organized MCS, and although it was poorly organized it still exhibited somewhat of a linear structure. At the same time, a smaller and weaker cluster of convection was progressing northeastward through central Iowa, likely driven by a warm front moving northward through the area. As the MCS approached far eastern South Dakota and southwest Minnesota a quasi-linear Type 3 CI event initiated in

southern Minnesota and along the Iowa/Minnesota border, connecting the MCS to the pre-existing convection that had continued to move northeast out of central Iowa (Fig. 4).

Surprisingly, even though Type 3 CI heavily depends on the linear system it is associated with, three of the four model runs produced the Type 3 CI in question even though the MCS's produced by those runs were fairly different (Fig. 20). As expected, the location of the initiation depended on the actual location of the MCS, but position of each of the three runs' pristine CI relative to their respective MCS's was quite consistent. In terms of reflectivity analysis, the only outlier was the run using the ACM2 scheme, which does not produce the observed Type 3 CI (Fig 20j-l). It is possible that this could be due to the location of the MCS produced in this run, which was significantly further north than what was simulated in the other three WRF runs. For initiation elevation, initiation in the RAP analyses takes place just below 700 hPa, or about 3000m AGL. Like what was seen in the 24 June Type 1 event, the models that captured the CI event approached saturation, and thus likely initiated convection at a lower level that what was observed in the RAP analyses. The QNSE PBL scheme was especially low, initiating convection near 1500m AGL. However, just like in the 24 June Type 1 case, these were the models that did produce the pristine CI event. The main difference in the run that didn't produce the event, the ACM2 PBL run, was a much dryer surface layer, with a slight inversion present above the layer that appears to approach saturation, which may have inhibited convection.

d. 26 June – Type 4

The final case modeled was a Type 4 case in extreme eastern Missouri. This case was a bit unique, in that it behaved somewhat like a Type 3 CI event since it was near an organized

MCS. However, it did not exhibit any sort of linear structure. In fact, the cells were almost evenly spaced ahead of the convection as well as its associated gust front. Due to these factors, as well as the lack of a frontal feature or boundary and no LLJ in the area, this event was classified as a Type 4 CI event. As stated, the event was in conjunction with an MCS that had formed out of a Type 1 CI event in northeast Kansas earlier in the night. That MCS slowly progressed through Kansas City, MO. After passing through Kansas City, a cluster of very small convective cells began to form just ahead of the MCS's outflow. This continued for about 2 hours, at which point the MCS begat to accelerate and overtook the area (Fig. 5).

In this Type 4 event, only two of the four PBL schemes, YSU and MYNN, produced the pristine CI event (Fig. 21a-c and 21g-i). In fact, the ACM2 scheme failed to capture the original Type 1 CI event that caused the MCS (Fig. 21j-l). Examination of the modeled soundings showed that the main difference between the two PBL schemes that failed to produce the Type 4 CI event and the two that did was a shallower elevated dry layer just above 700 hPa in the models that did not produce the pristine CI event. While all four model runs tended to be a bit shallower than what was observed, the two that failed to capture the event (the QNSE and ACM2 PBL schemes) were the shallower two.

3.5 Conclusions and discussions

A general climatology of pristine nocturnal CI was completed for 287 initiation events during May, June, July, and August 2015 to distinguish any apparent trends and tendencies that may help increase forecasting skill. Knowledge of general trends may also allow National Weather Service offices to better anticipate convective initiation and set staffing levels accordingly. The climatology was performed over a large domain, encompassing all

the United States Great Plains region, from central Texas to the Canadian border. Analyses of timing of the initiation revealed that one major peak exists, occurring near 0400 UTC, with an additional less prominent peak occurring during the 0700 UTC – 0800 UTC period. This is suggestive of a couple of things. One possibility is that the peaks are caused by the strengthening and subsequent weakening of the LLJ over time, since there seems to be a relative minimum around the time when the LLJ would typically be at a maximum. If this were the case, then Type 1 and Type 2 CI would be expected to dominate the occurrences in these peaks. When separating the events into the four different types, evidence of the LLJ driven hypothesis for the twin peaks does appear evident, as Type 1 and Type 2 tend to dominate both peaks. However, when all CI is split even further into the three subdomains, the LLJ explanation starts to fall apart, depending on the subdomain. While the Upper Plains domain does appear to still exhibit some dependence on LLJ evolution, due to peaks showing up at different times for each PNCI type, the PECAN subdomain has dual peak structures at the same time for *all* PNCI types, which in turn matches the overall PNCI peaks, suggesting something other than the LLJ was causing the dual peak structure. What this factor would be is still a bit nebulous at this point, but is important for forecasting PNCI. In turn, another possibility may be that some factor might not necessarily be driving the dual peaks, but may be *surprising* initiation in the valley that occurs between the two peaks.

Magnitude of elevation of each type of PNCI was thought to play an important role in how and why each type formed, thus two different methods were used to gain a general understanding of how elevated each type of PNCI was. However, each method produced quite different results. The most drastic difference between the two was the MUCAPE/MLCAPE method (the simplest and quickest to perform) showing Type 3 PNCI

being the *least* elevated type, while the sounding method (the most accurate) showed Type 3 PNCI to be the *most* elevated type. Since the first method uses how elevated the MUCAPE was to show at what level initiation was occurring, the fact that this method was not matching *actual* analysis of soundings for each event means that much of these events are likely not being initiated where the most unstable CAPE was residing. Therefore, it could be assumed that they are taking place at the level where the least CIN is, meaning forecasting location of PNCI may rely more on understanding of CIN at different levels of the atmosphere than it does on CAPE.

High resolution models used during the PECAN field campaign were analyzed to identify any trends for predicting PNCI. Through this analysis, the LLJ driven PNCI types (1 and 2) appeared to be better predicted in location than Types 3 and 4. Since Type 3 is completely dependent on the location of the parent MCS, thus correct prediction of Type 3 initiation can only occur if the parent MCS is also correctly predicted, which lends to a heightened level of uncertainty. Subsequently, the nature of Type 4 lends itself to be less predictable, since this type occurs without obvious forcing mechanisms. An additional factor to consider is the elevation levels of each type of PNCI. Ignoring Type 4 and its intrinsic uncertainties that come with it, the worse-predicted types of PNCI appear to also be the most elevated, especially when considering that the type that was most common to be *completely* missed by the high resolution PECAN models was Type 2, which was the second most elevated type after sounding analysis (Table 2 and 3). However, performing 90% and 95% significance level T tests showed that there was no significant difference in model handling of CI location between types.

Further examining model handling of elevation level of each type of PNCI, four versions of a 4km WRF-ARW model were run for four cases during the study period, one for each PNCI type. Analysis found that, while many of the models tended to initiate convection at a lower elevation than what was observed in the RAP analyses used for comparison to real world observations, convection still initiated and in relatively the correct spot (or, in the case of Type 3, relatively the same spot in relation to wherever the parent MCS was). As was seen several times in the PECAN model verification, every version of the WRF model run for the Type 2 case failed to produce the convection. Perhaps, in the case of Type 2, smaller scale features or impulses moving through the LLJ are causing the initiation, rather than the LLJ itself. If the occurrence of these small scale features, whether they be features like gravity waves or moisture fluctuations within the jet, is relatively hard to predict, that could explain why for those Type 2 events that *are* predicted to occur are relatively well predicted, while other events catastrophically fail.

Overall, all four types of PNCI seem to be heavily dependent on small factors/changes in the atmosphere, which can be seen by the failure of the ACM2 model to predict the Type 1 case on 24 June. While all other boundary layer parameterizations for that day predicted the event remarkably well, the ACM2 completely failed to produce the PNCI event even though its profile was only marginally different from the other models and the observed RAP analyses. Further research will be needed to determine the extent that this type of convective initiation relies on features smaller than the mesoscale, how sensitive initiation is to the occurrence or absence of these features, as well as if these features play a role in the dual peaked structure seen in some areas of the plains when considering what time of night most PNCI occurs.

3.6 Acknowledgements

This research was supported primarily by National Science Foundation grant AGS1359606. The author would like to thank everyone involved with the PECAN field campaign, especially those managing the website that houses the archived model output used for the model verification section.

3.8 Tables

Table 1: Physics package used for the four WRF-ARW simulations that examine sensitivity to choice of PBL scheme (PBL schemes tested are described in text).

Microphysics	Morrison
Longwave Radiation	New Goddard
Shortwave Radiation	New Goddard
Land Surface	Noah Land Surface Model
Cumulus Parameterization	None
Urban Surface	Urban Canopy Model

Table 2: Hit rate, false alarm rate, and threat score for each of the high resolution PECAN models.

	NSSL WRF	**MPAS**	**WRF-MAP**	**NCEP HRRRv1**	**CSU WRF**
Hit Rate	52%	58%	57%	39%	64%
False Alarm Rate	65%	49%	59%	64%	51%
Threat Score	27%	38%	31%	23%	38%

Table 3: Model verification of June PNCI events. Cells shaded in red and with an "X" indicate the model did *not* produce the observed initiation. N/A show cases where the observed initiation occurred outside the archived model's domain or the archived image was unavailable.

PNCI Type	NSSL WRF	MPAS	WRF-MAP	NCEP HRRRv1	CSU WRF
1	n/a	n/a	n/a	n/a	X
1	n/a	n/a			
1					
1	n/a				
1	n/a				
1		X			X
1	n/a				
1					
1		X	X	X	
2	n/a	n/a	n/a	n/a	n/a
2	n/a	n/a	n/a	X	
2	n/a	n/a			
2	n/a	n/a		n/a	
2	n/a	n/a			X
2	n/a	n/a	X		X
2	n/a	n/a	X	n/a	
2	n/a	n/a	X	X	
2	n/a	n/a	X		X
2	n/a	X	X	n/a	
2	n/a		X	n/a	
2	n/a			X	
2	n/a				
2	X		X	n/a	
2	X	X	X		X
2		X	X	X	X
2	n/a	X	X	n/a	X
2	n/a	X		n/a	
2	n/a		X		X
2	X	X		X	X
3	n/a	n/a	n/a	X	X
3	n/a			X	
3	n/a			X	
3	n/a		n/a	n/a	
3	n/a	X		n/a	X
4					
4	X	n/a	X	X	
4		X	X	n/a	

Table 4: As in Table 2 except for July PNCI events.

PNCI Type	NSSL WRF	MPAS	WRF-MAP	NCEP HRRRv1	CSU WRF
1	n/a		X	X	
1	n/a	n/a		X	
1				X	
1	X	X		X	
1	X	n/a	X	X	X
1		n/a			X
1	n/a	n/a		X	
2	n/a	n/a	X	n/a	
2			X	X	
2	X	X	X	X	X
2				X	
2		X		X	
2	X	X	X	X	X
2	n/a	n/a	X	X	X
2	n/a	X	n/a	n/a	X
2	n/a	n/a	X	X	X
2	n/a		n/a	X	
2	X	n/a			
3	X	n/a		X	X
3		n/a		X	
4	X	n/a	X		X
4	n/a			X	
4	X			X	

3.9 Figures

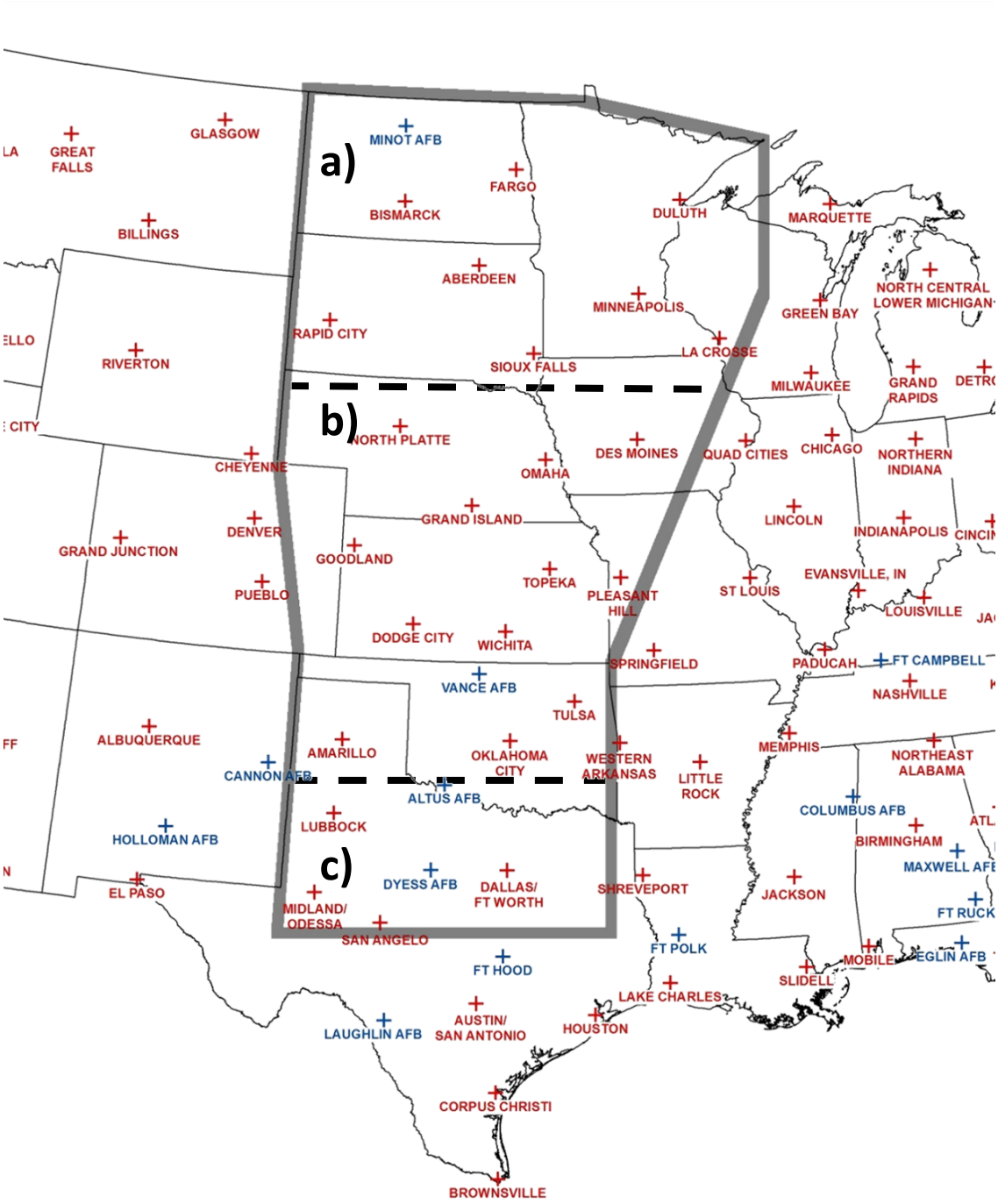

Figure 1: Full domain for this study (solid grey) including the WSR-88D radars used, along with subdomains (separated by dashed lines) for a) Upper Plains, b) PECAN, and c) Texas.

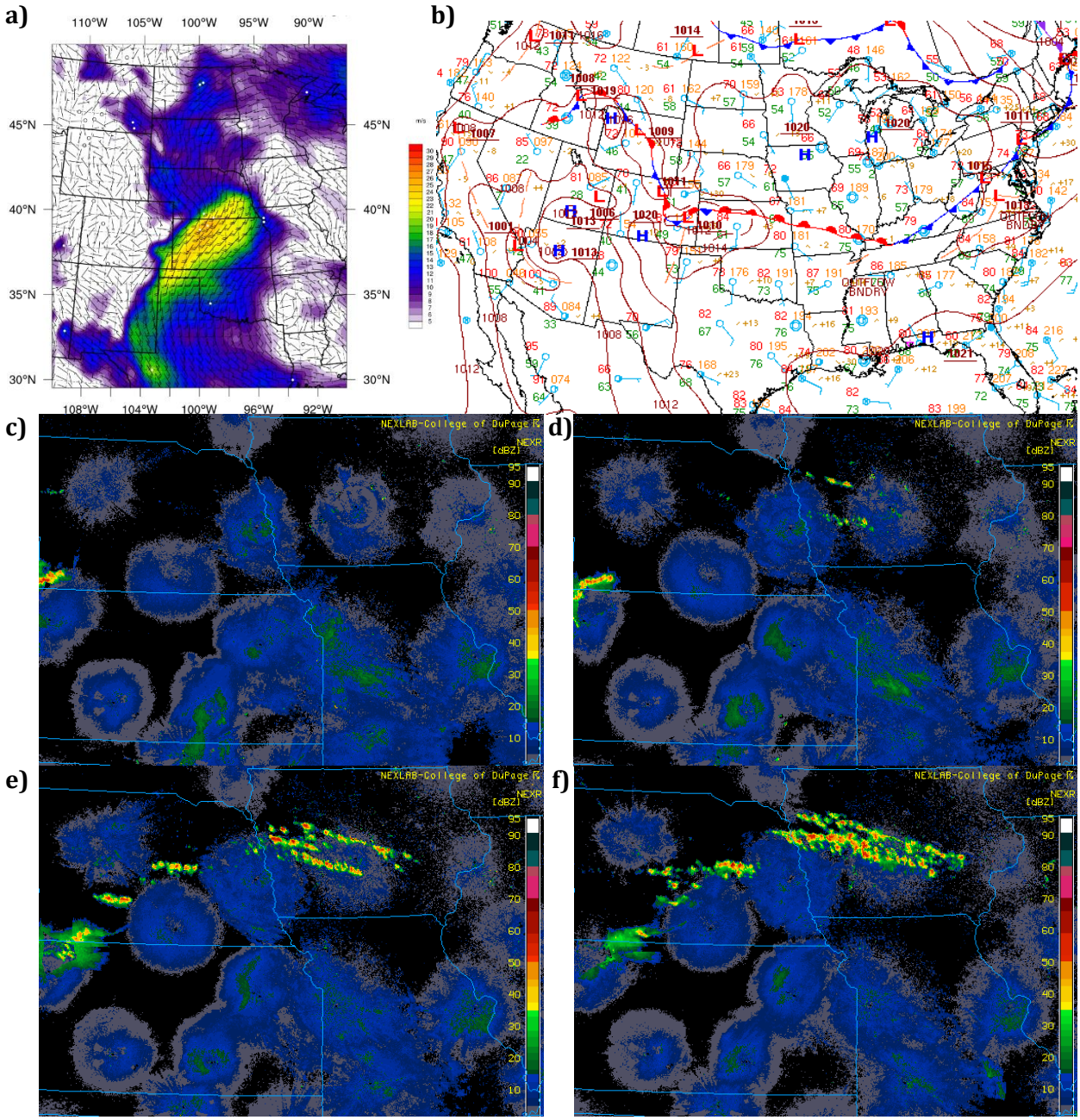

Figure 2: 24 Jun a) LLJ magnitude (contoured from 5 to 30 ms^{-1}, every 1 ms^{-1}) and wind barbs at 850mb for 0500 UTC, b) WPC surface map analyzed at 0300 UTC, and radar reflectivity at c) 0400 UTC, d) 0500 UTC, e) 0600 UTC, and f) 0700 UTC, with color bars on the right hand side of each sub-figure.

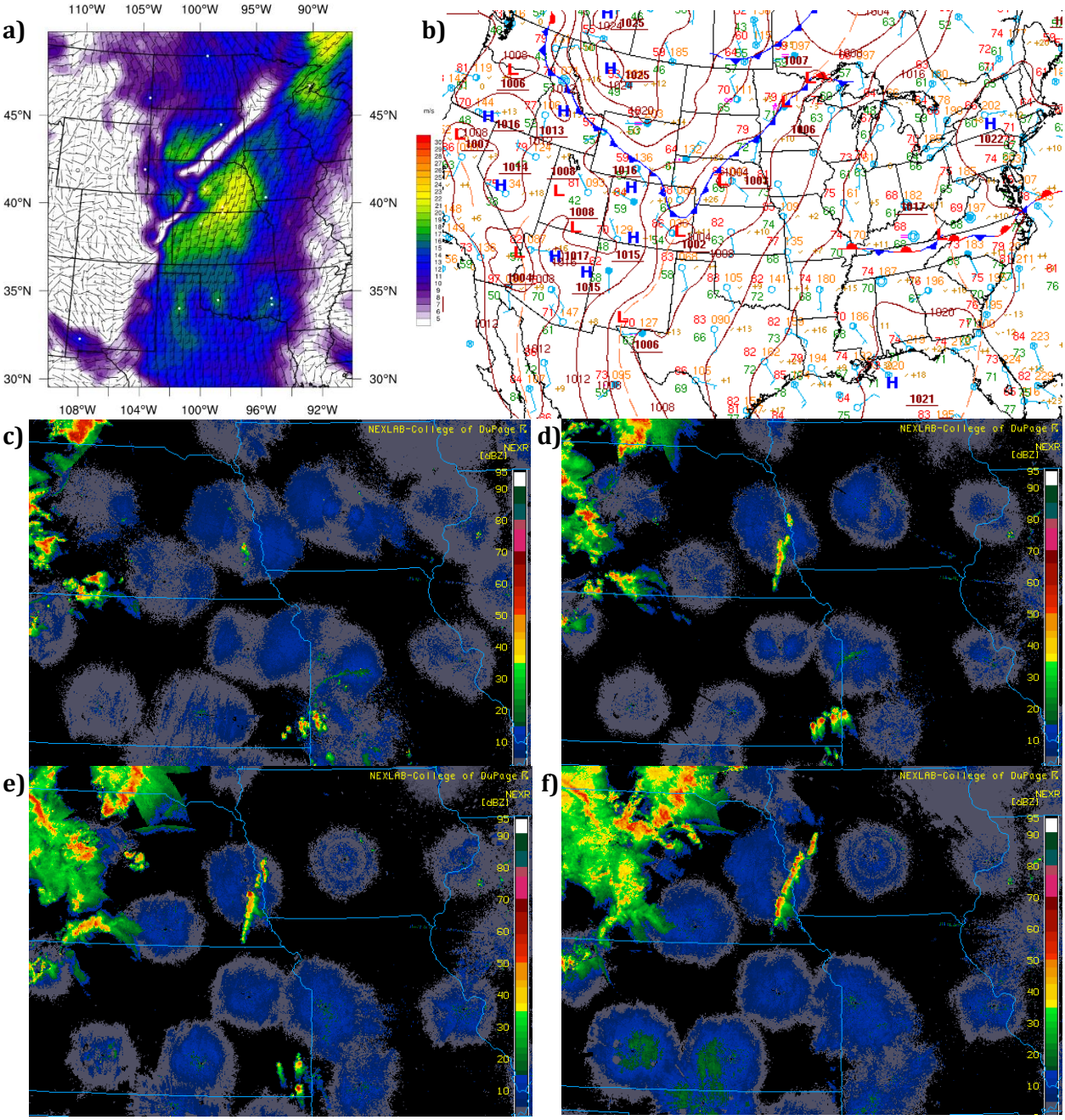

Figure 3: 6 Jul a) LLJ magnitude (contoured from 5 to 30 ms^{-1}, every 1 ms^{-1}) and wind barbs at 850mb for 0300 UTC, b) WPC surface map analyzed at 0300 UTC, and radar reflectivity at c) 0100 UTC, d) 0200 UTC, e) 0300 UTC, and f) 0400 UTC, with color bars on the right hand side of each sub-figure.

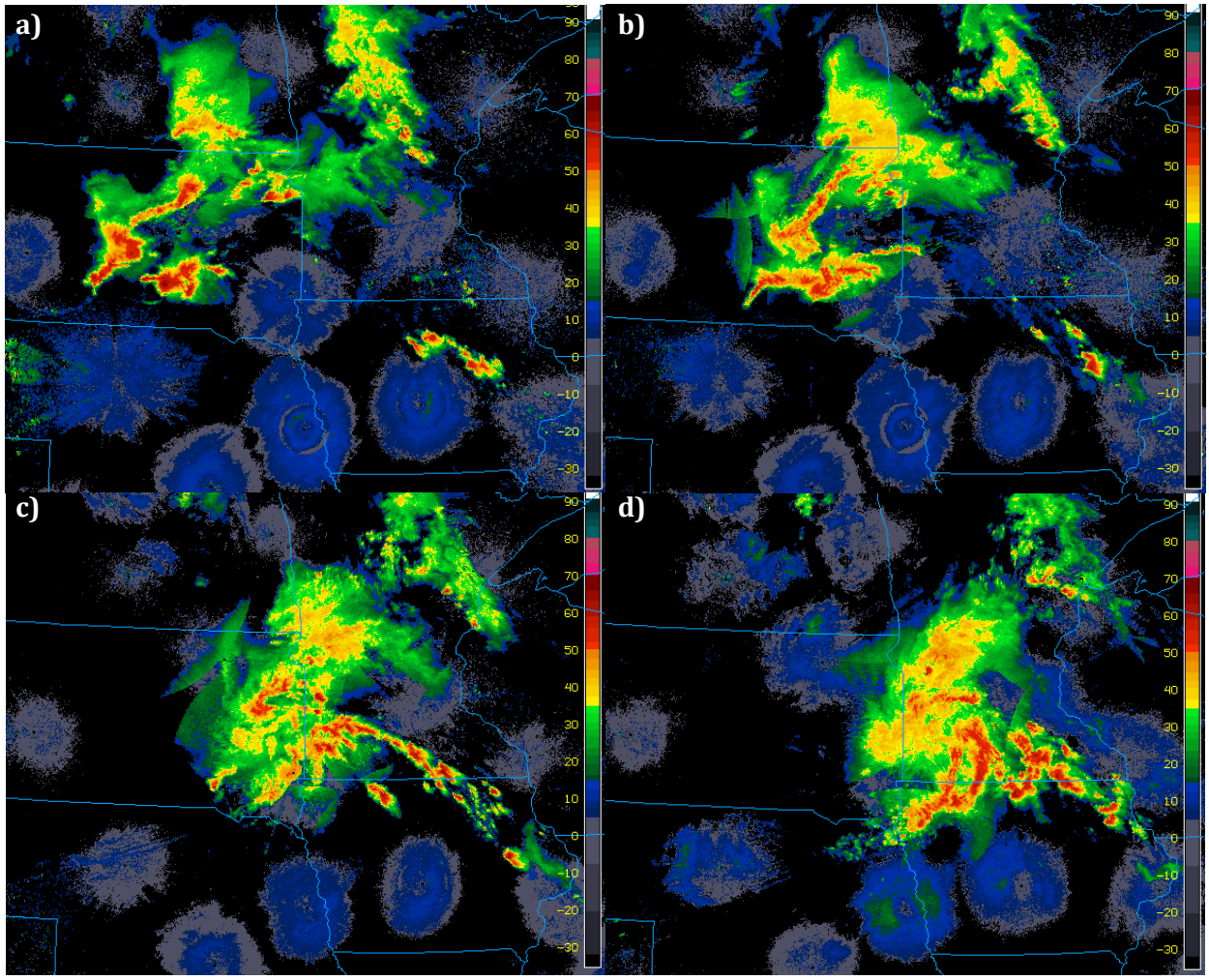

Figure 4: 28 Jul radar reflectivity at a) 0400 UTC, b) 0500 UTC, c) 0600 UTC, and d) 0700 UTC, with color bars on the right hand side of each sub-figure.

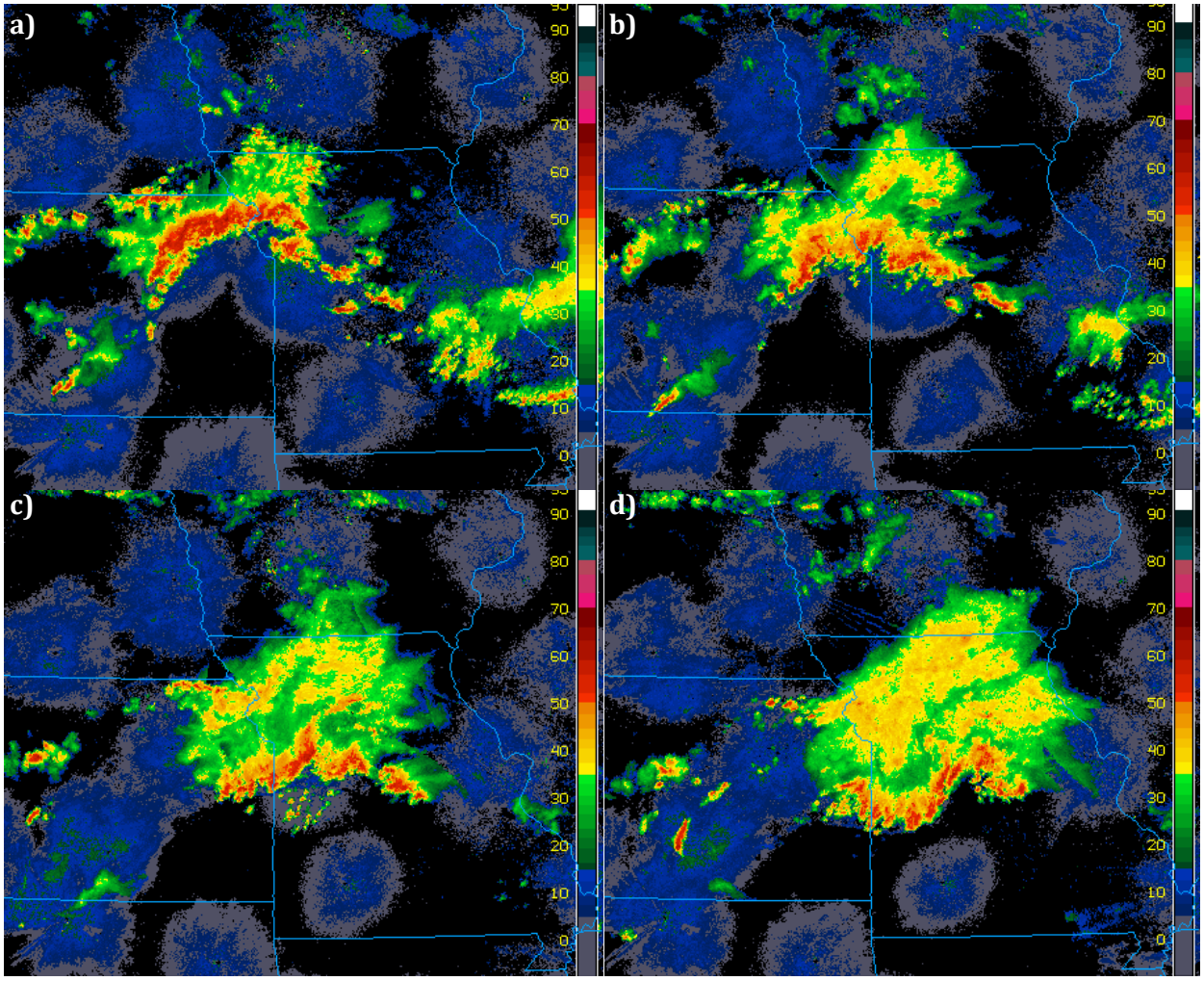

Figure 5: 26 Jun radar reflectivity at a) 0530 UTC, b) 0630 UTC, c) 0730 UTC, and d) 0830 UTC, with color bars on the right hand side of each sub-figure.

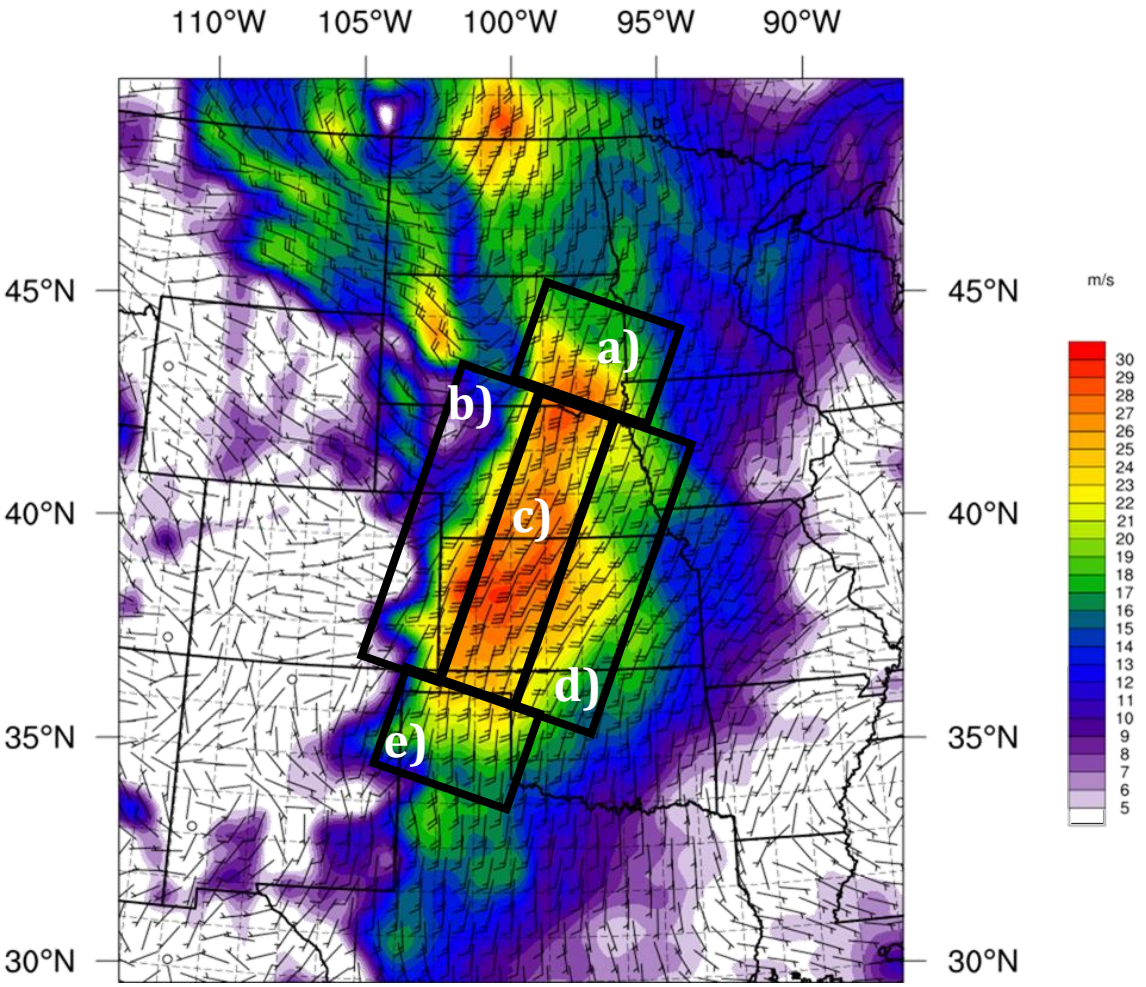

Figure 6: Example (28 Jul) of the subgroups of Type 2 PNCI: a) Nose, b) Left, c) Middle, d) Right, and e) Tail

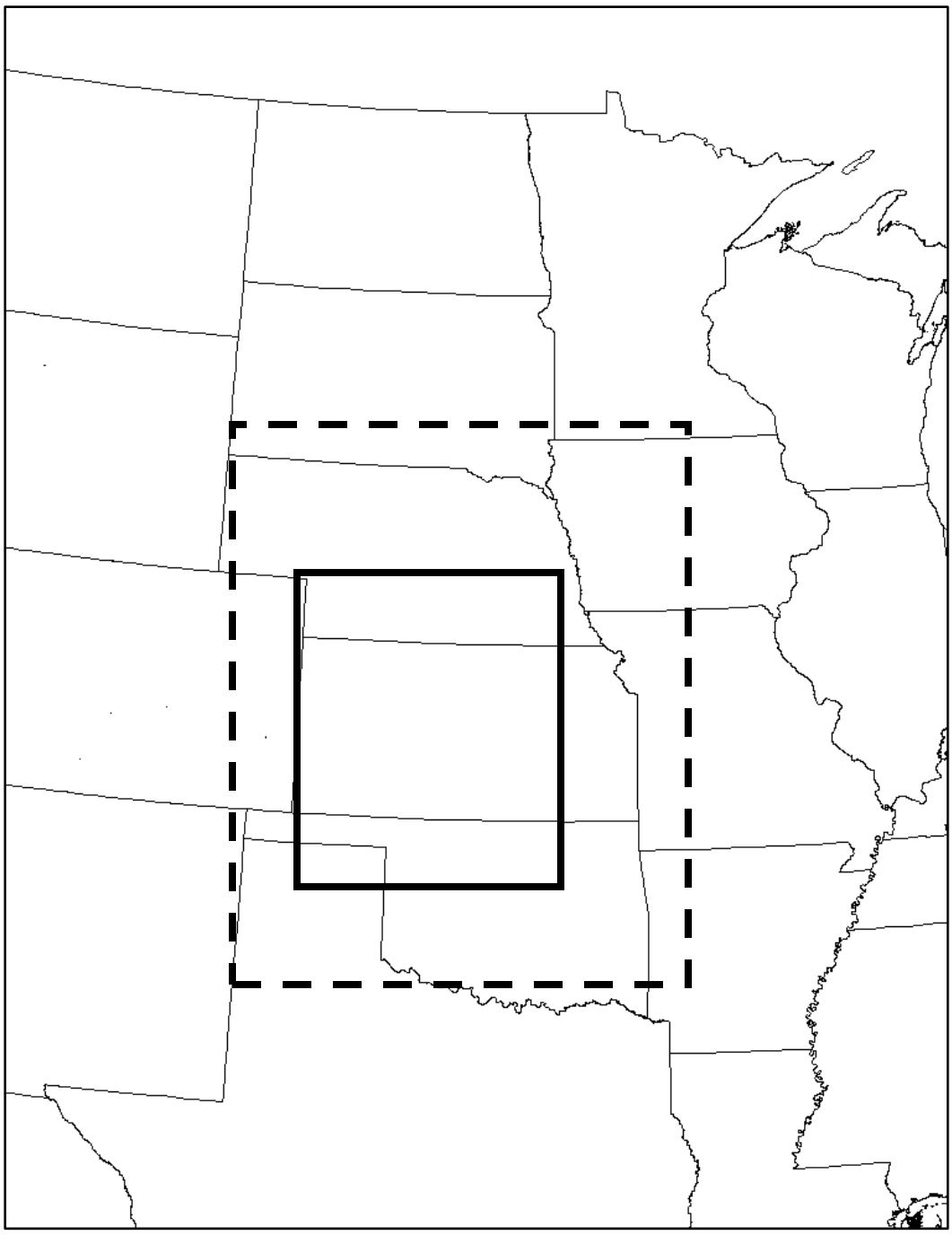

Figure 7: The original PECAN domain (solid line) and the effective PECAN domain (dashed line) used for the model verification portion of this study.

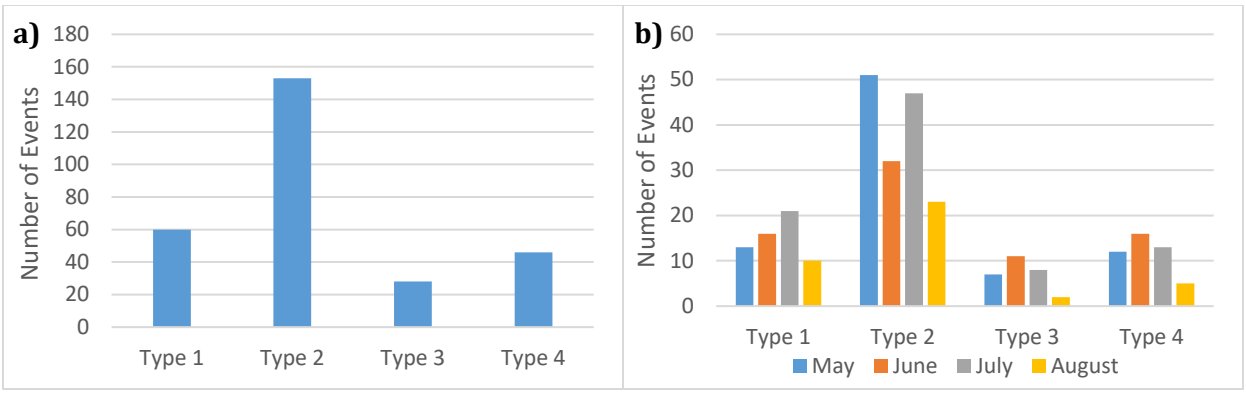

Figure 8: Overall NCPI frequency by a) type only and b) type and month

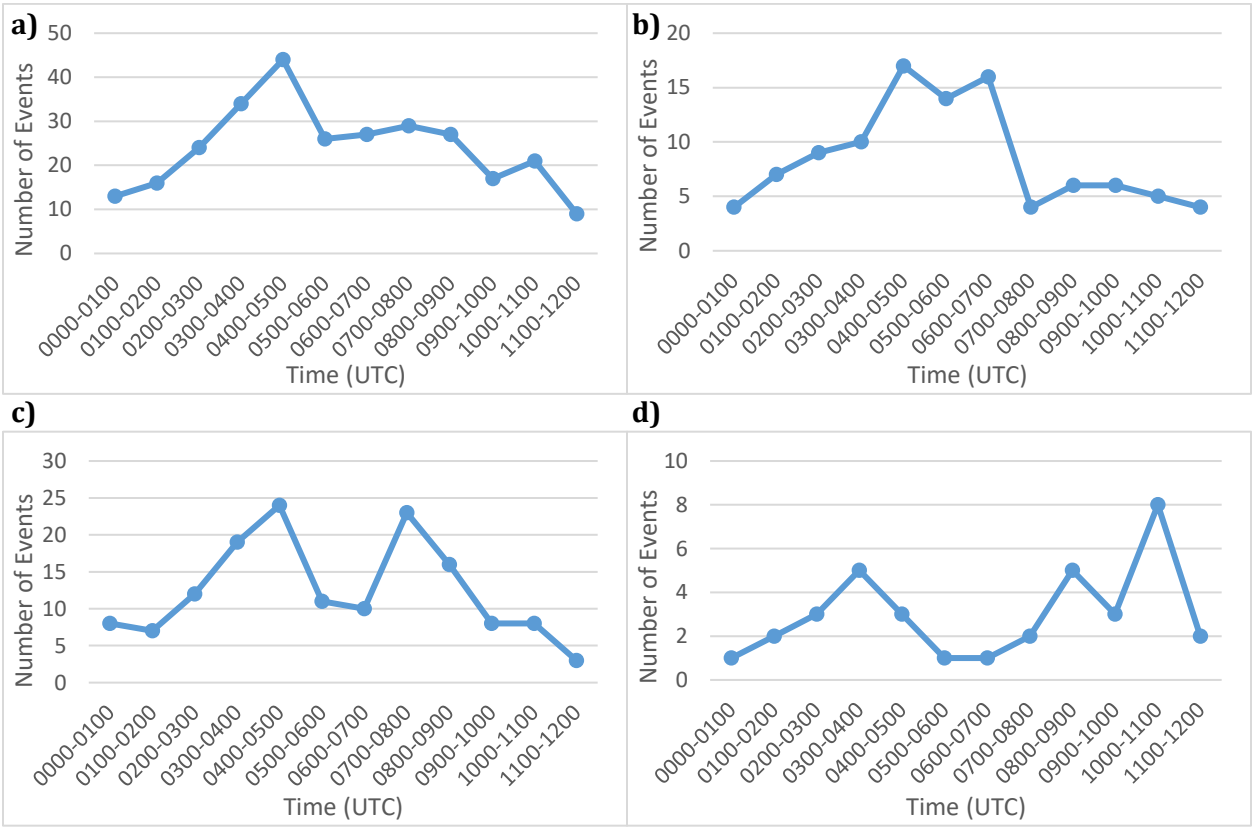

Figure 9: Frequency of PNCI over time, for the a) entire domain, b) Upper Plains subdomain, c) PECAN subdomain, and d) Texas subdomain

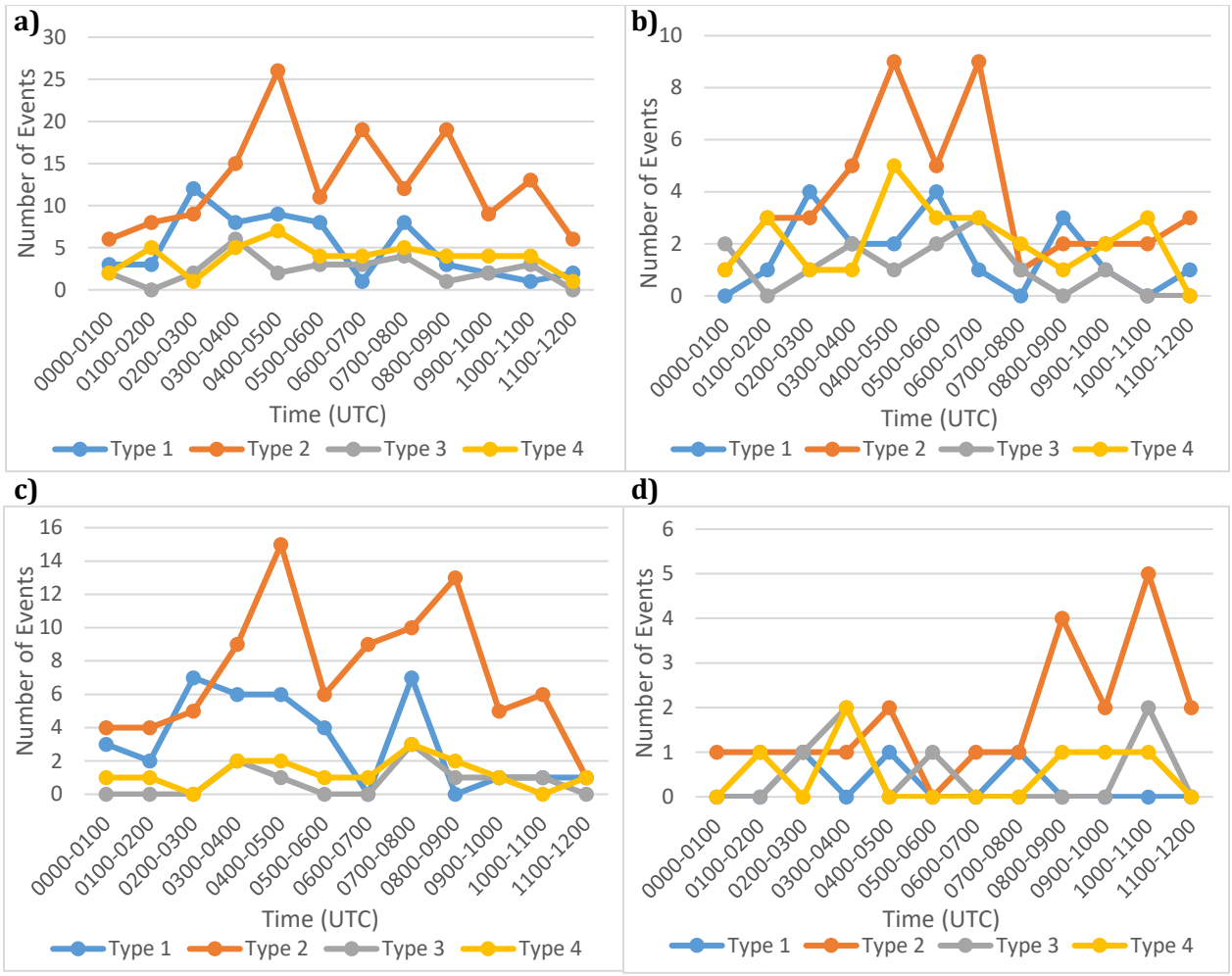

Figure 10: Frequency of PNCI over time, by PNCI type, for the a) entire domain, b) Upper Plains Subdomain, c) PECAN Subdomain, and d) Texas Subdomain

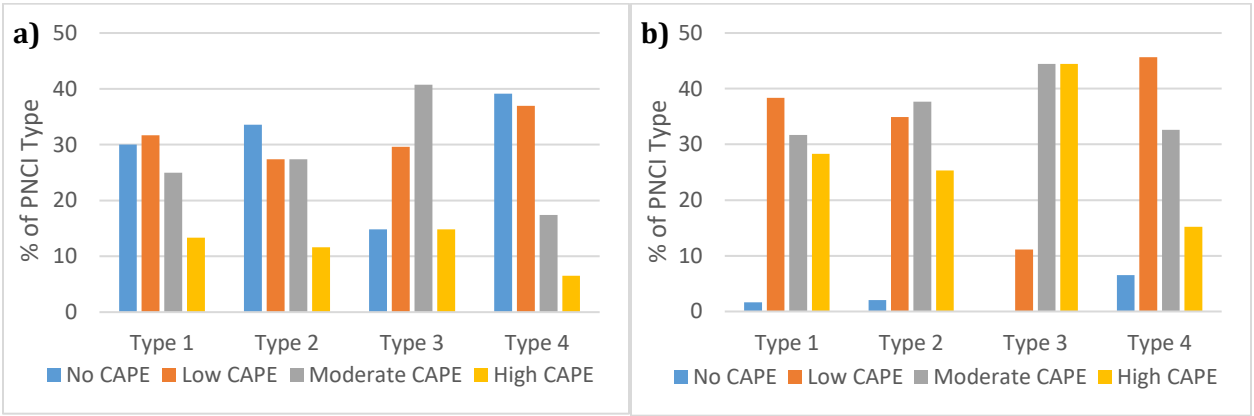

Figure 11: Percentage of each PNCI type in each CAPE threshold, for a) MLCAPE and b) MUCAPE

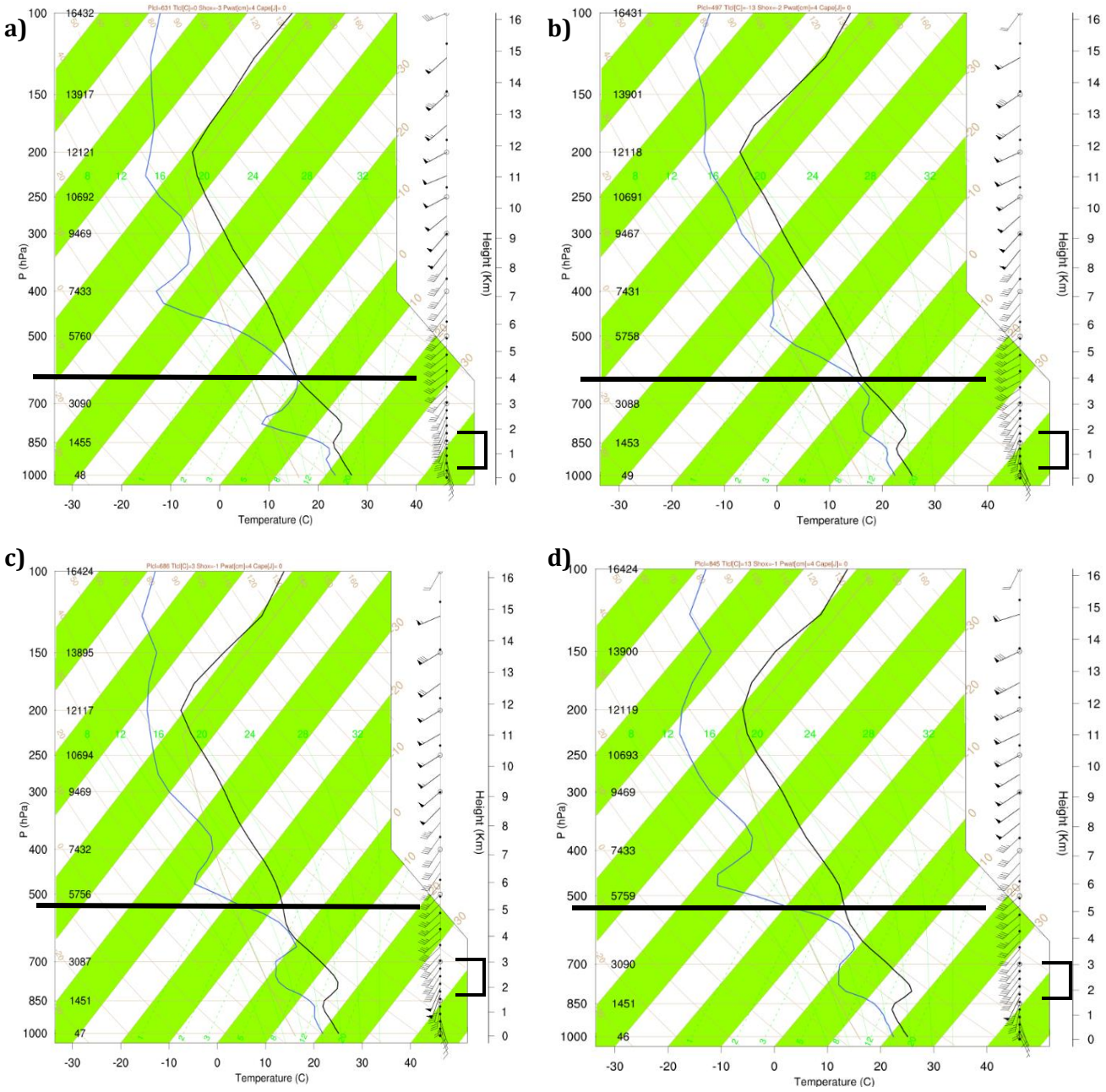

Figure 12: RAP analysis soundings for 16 May, southeast of Lubbock, TX at a) 0800 UTC, b) 0900 UTC, c) 1000 UTC, and d) 1100 UTC, showing initiation taking place at about 4000m AGL (black line), well above the approximate elevation of the LLJ (black bracket on right).

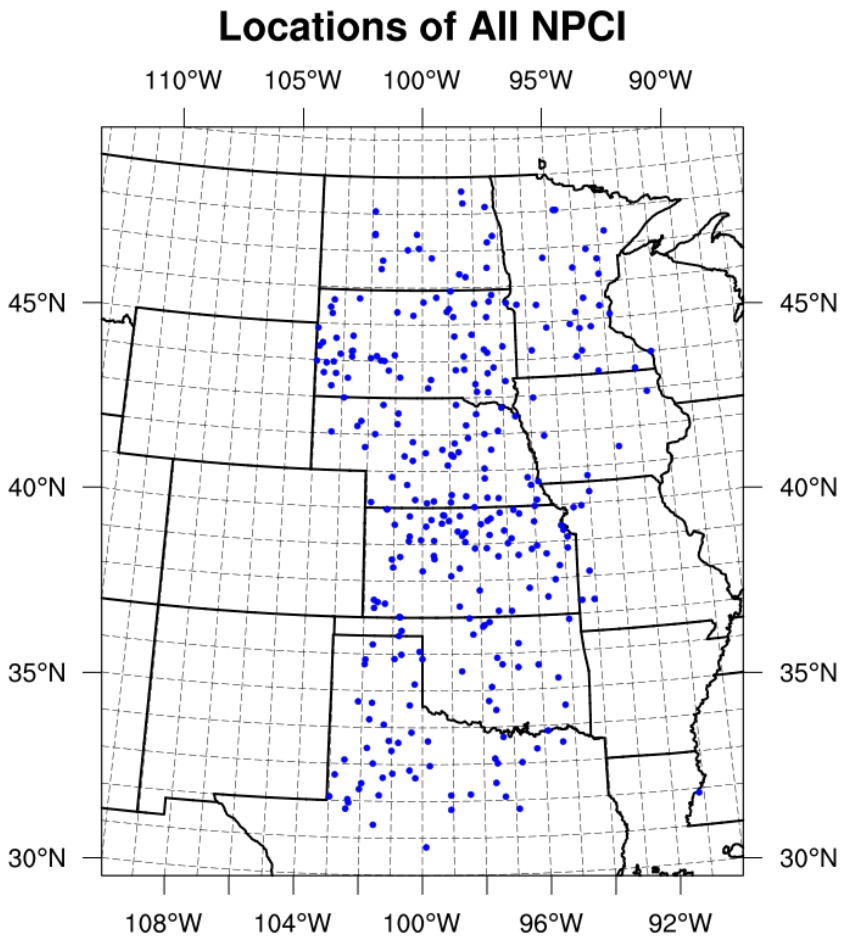

Figure 13: Locations of all PNCI events over the entire study period

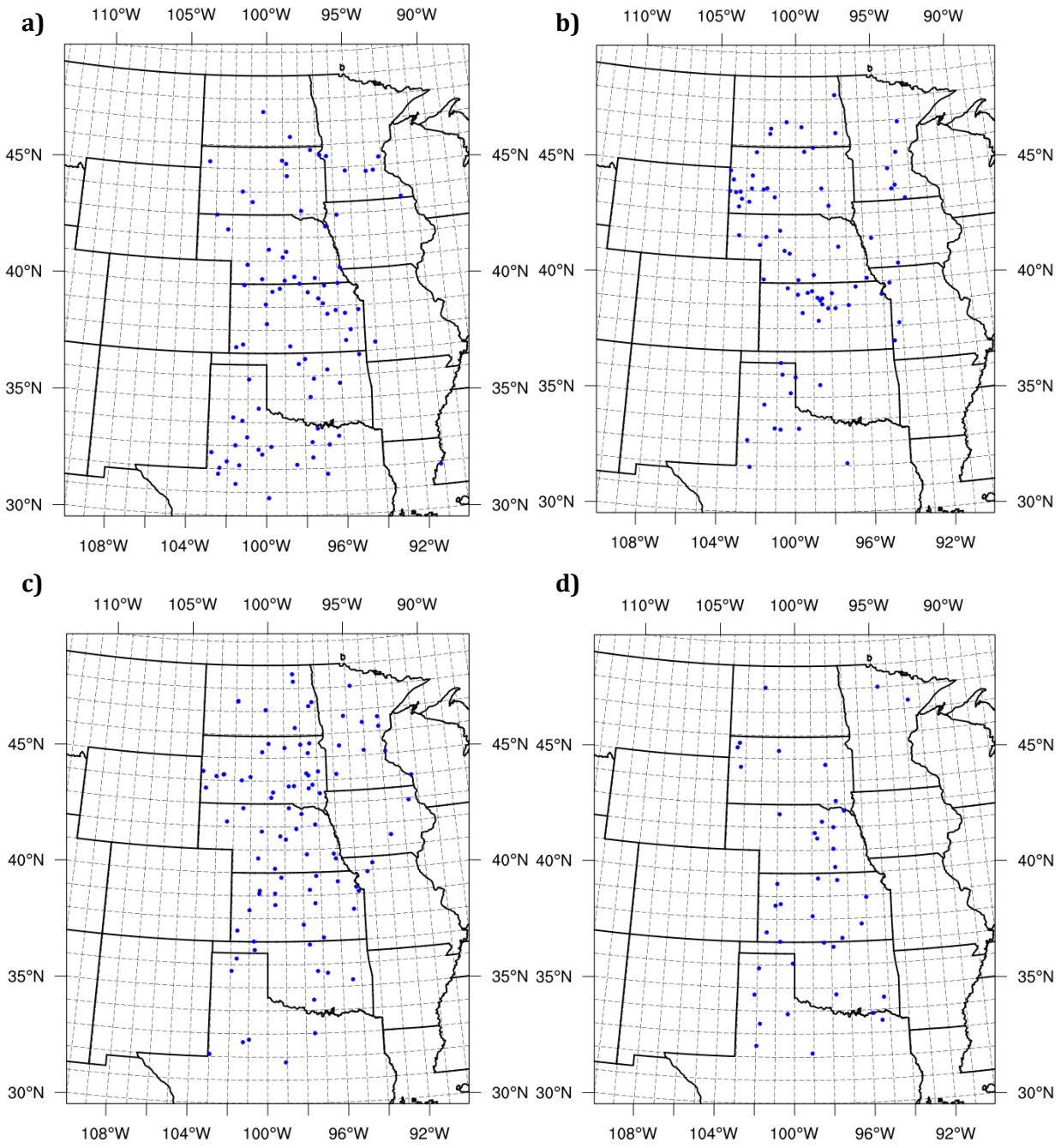

Figure 14: Locations of all PNCI types, split by month: a) May b) June c) July and d) August

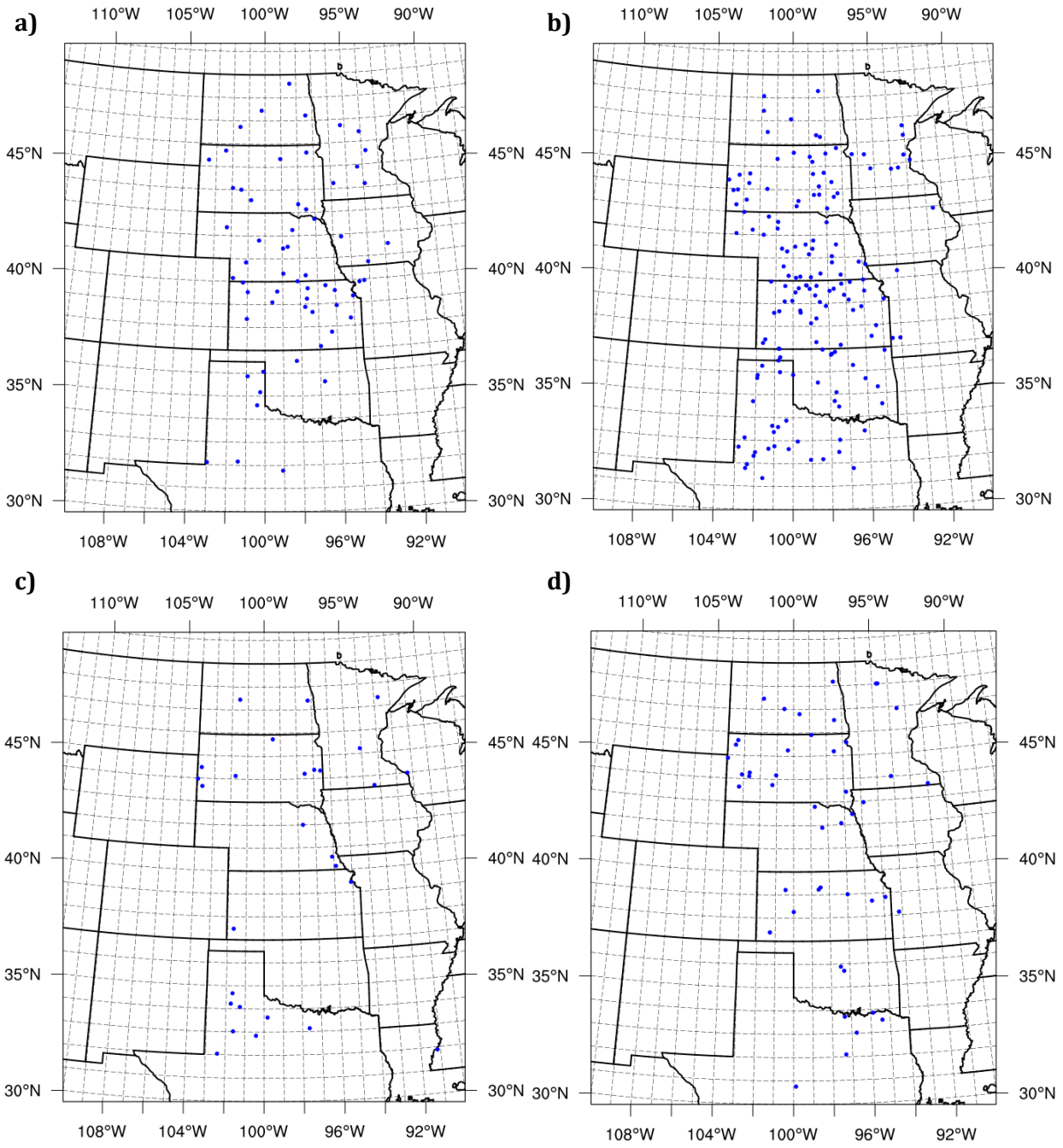

Figure 15: Locations of each PNCI type over the entire period: a) Type 1 b) Type 2 c) Type 3 and d) Type 4

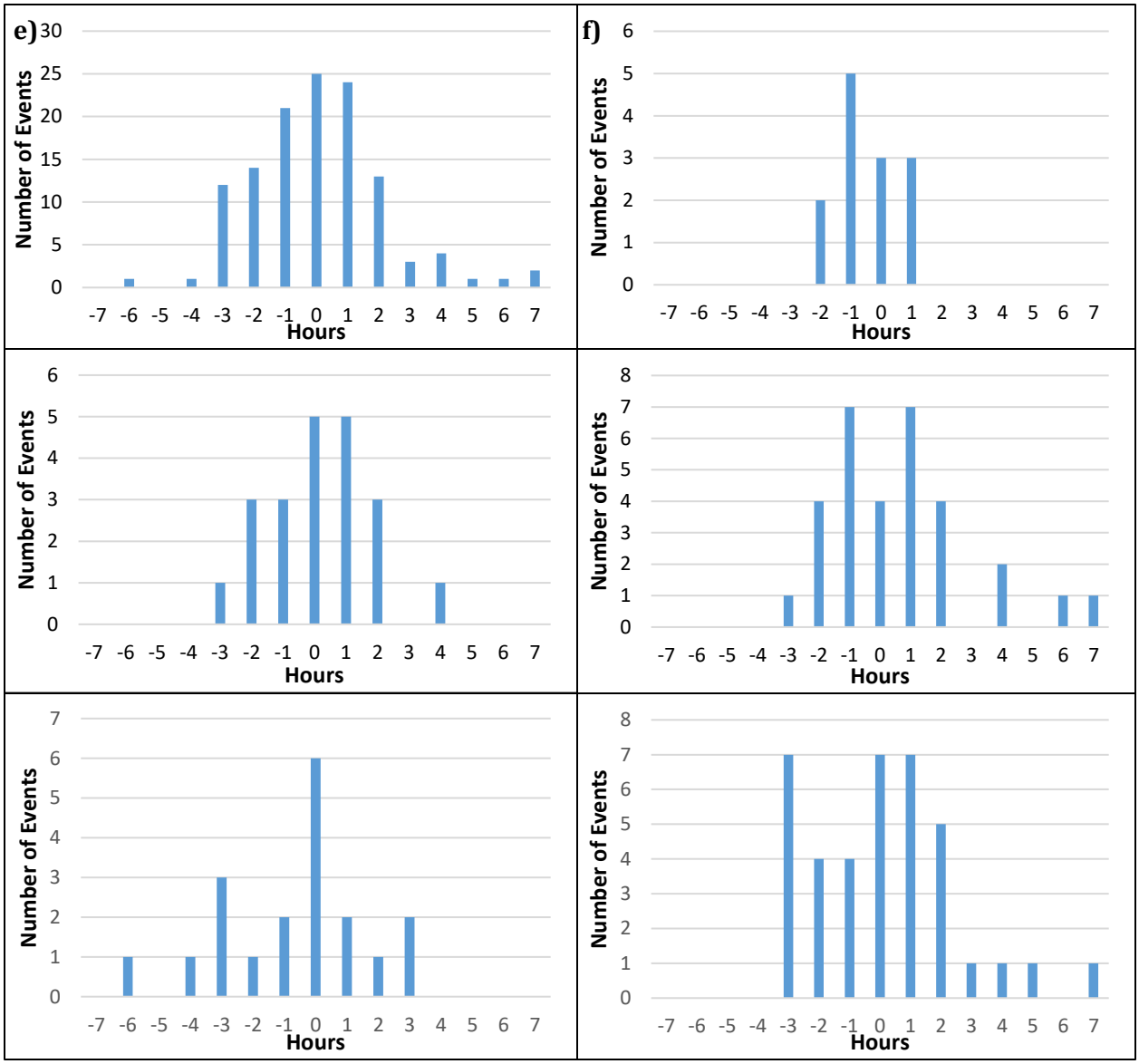

Figure 16: Absolute time error for a) all 5 high resolution models, b) NSSL WRF, c) MPAS, d) WRF-MAP, e) NCEP HRRRv1, and f) CSU WRF. Negative numbers indicate convection triggered early, while positive numbers indicate it triggered late.

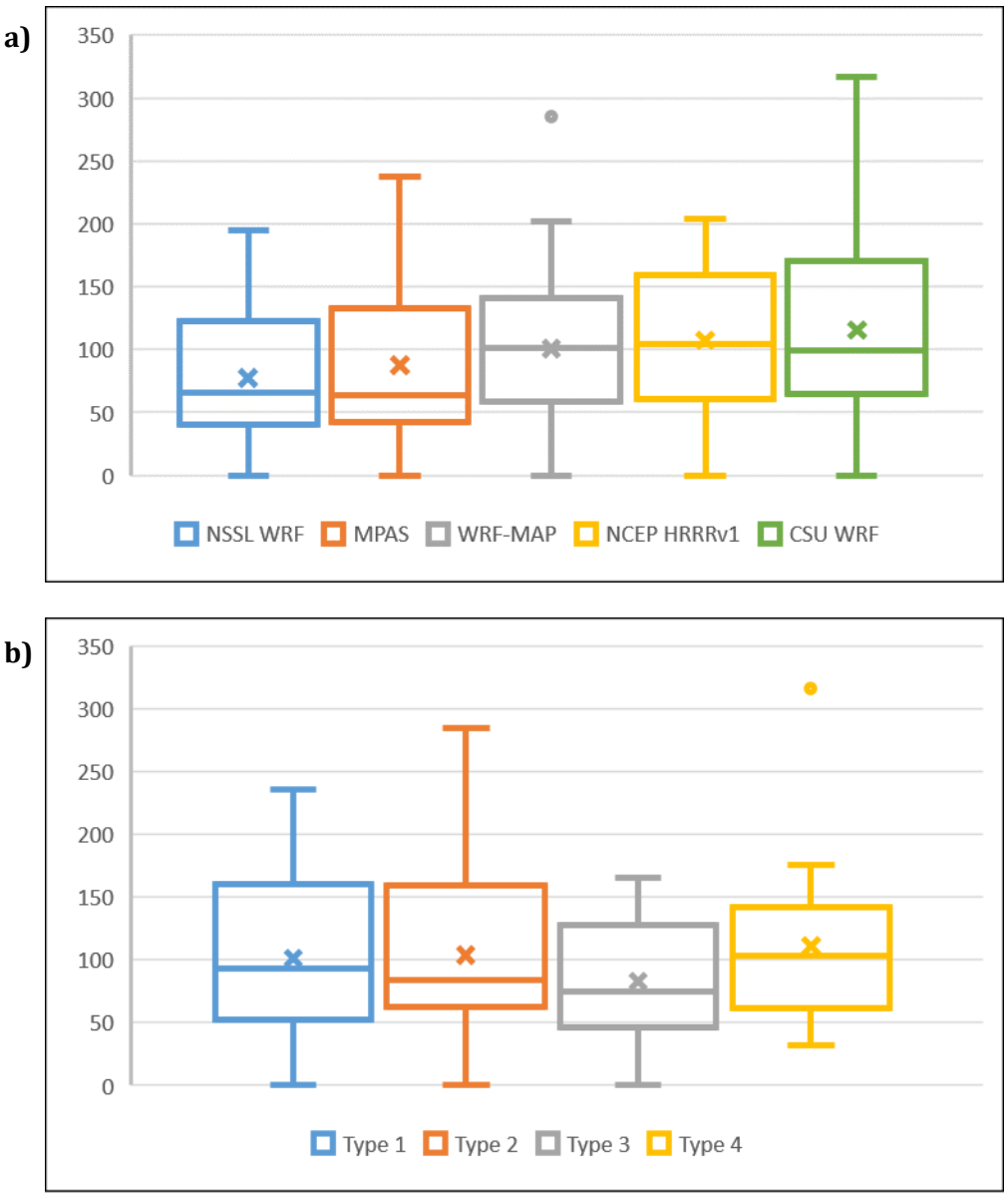

Figure 17: Box plots of mean absolute error of distance in km for a) each of the 5 PECAN CAMs and b) each PNCI type.

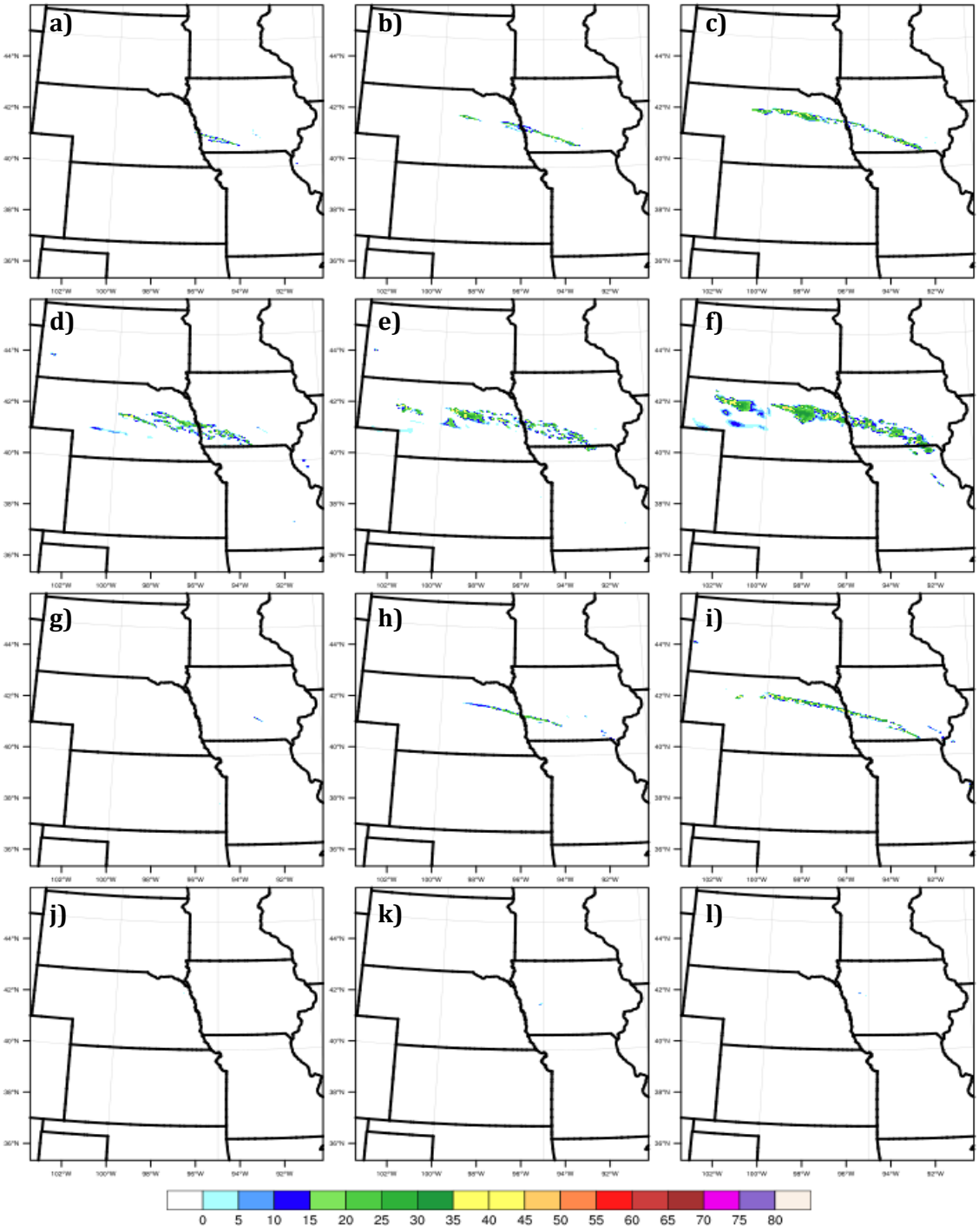

Figure 18: Simulated reflectivity for 24 June for the YSU scheme at a) 0600 UTC, b) 0700 UTC, and c) 0800 UTC, the QNSE scheme at d) 0600 UTC, e) 0700 UTC, and f) 0800 UTC, the MYNN scheme at g) 0600 UTC, h) 0700 UTC, and i) 0800 UTC, and the ACM2 scheme at j) 0600 UTC, k) 0700 UTC, and l) 0800 UTC.

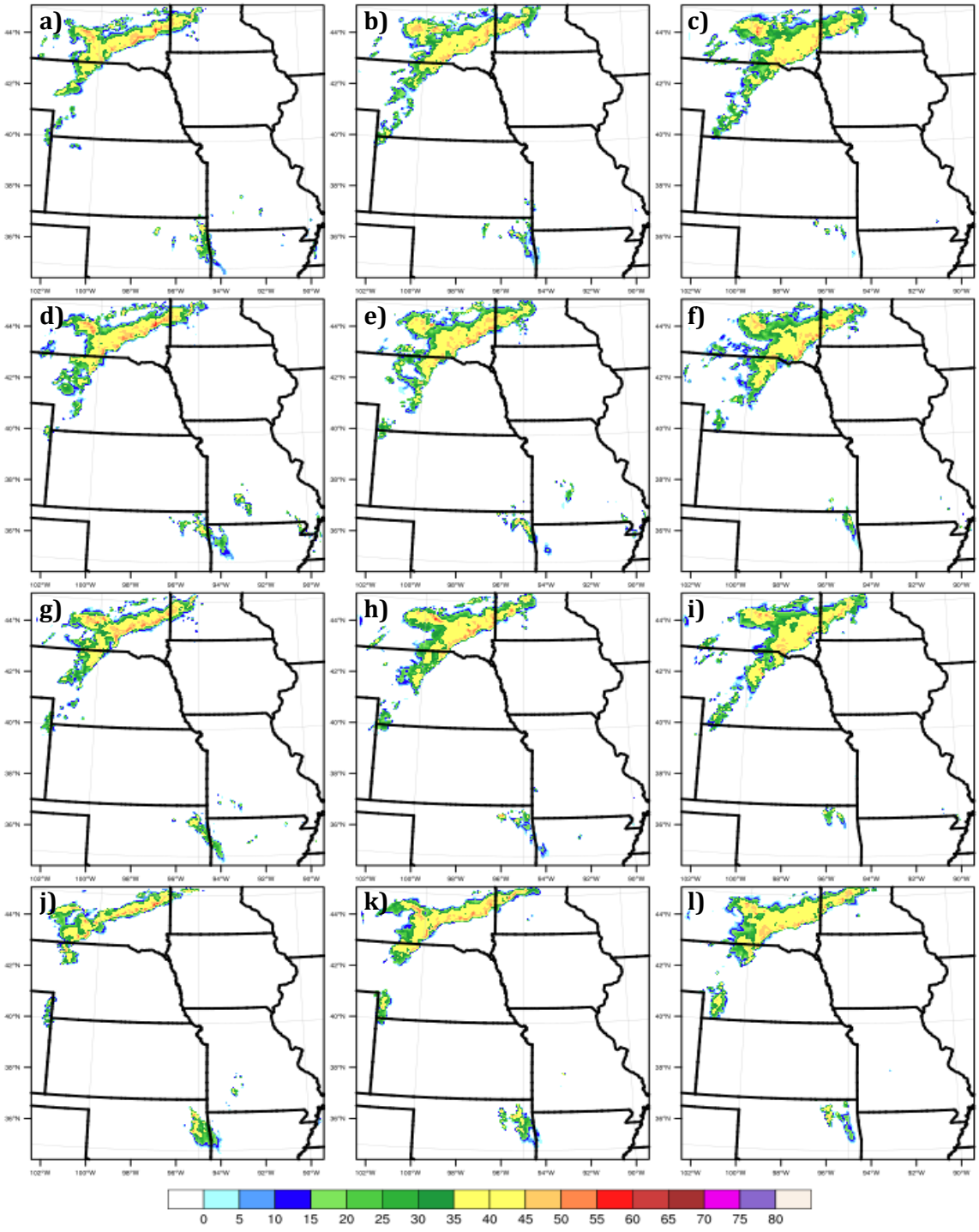

Figure 19: Simulated reflectivity for 6 July for the YSU scheme at a) 0200 UTC, b) 0300 UTC, and c) 0400 UTC, the QNSE scheme at d) 0200 UTC, e) 0300 UTC, and f) 0400 UTC, the MYNN scheme at g) 0200 UTC, h) 0300 UTC, and i) 0400 UTC, and the ACM2 scheme at j) 0200 UTC, k) 0300 UTC, and l) 0400 UTC.

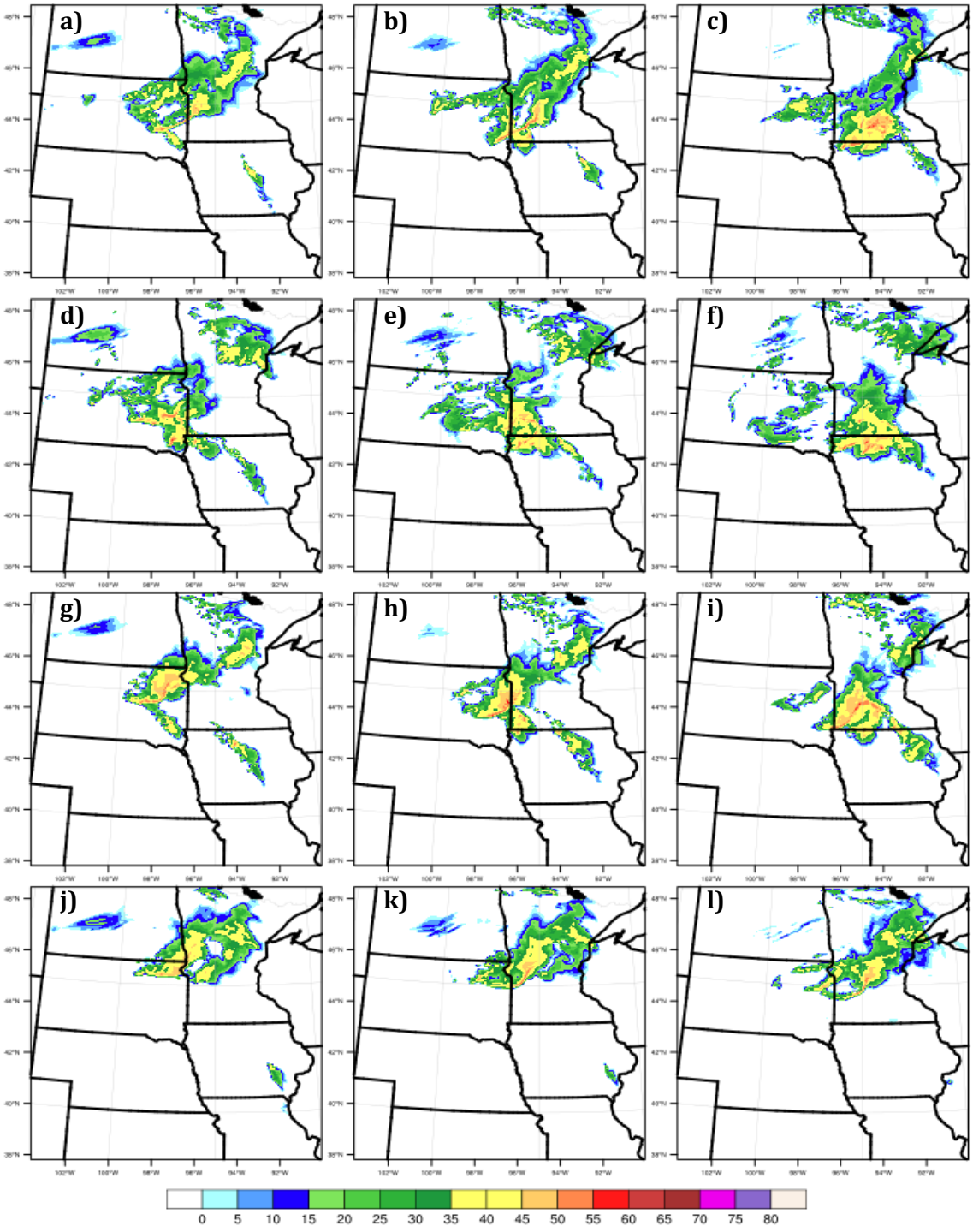

Figure 20: Simulated reflectivity for 22 June for the YSU scheme at a) 0900 UTC, b)1000 UTC, and c) 1100 UTC, the QNSE scheme at d) 0900 UTC, e) 1000 UTC, and f) 1100 UTC, the MYNN scheme at g) 0900 UTC, h) 1000 UTC, and i) 1100 UTC, and the ACM2 scheme at j) 0900 UTC, k) 1000 UTC, and l) 1100 UTC.

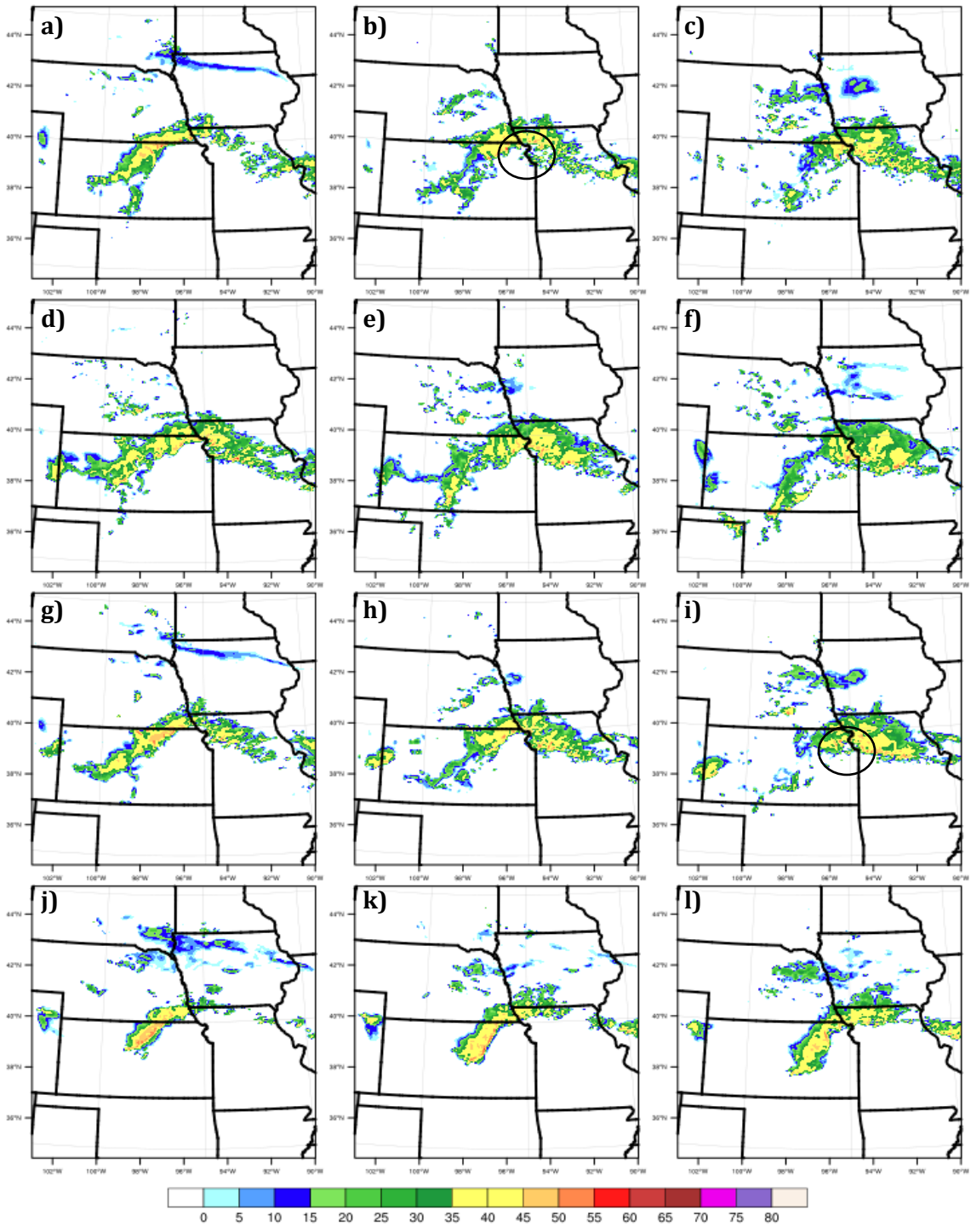

Figure 21: Simulated reflectivity for 26 June for the YSU scheme at a) 0630 UTC, b) 0730 UTC, and c) 0830 UTC, the QNSE scheme at d) 0630 UTC, e) 0730 UTC, and f) 0830 UTC, the MYNN scheme at g) 0630 UTC, h) 0730 UTC, and i) 0830 UTC, and the ACM2 scheme at j) 0630 UTC, k) 0730 UTC, and l) 0830 UTC. The small areas of interest for the YSU and MYNN schemes are circled.

CHAPTER 4. GENERAL CONCLUSIONS

The main purpose for this project was to identify both spatial and temporal trends in the occurrence of four different types of PNCI and to study if predictability of the different types varies in convection allowing models run during the PECAN field campaign. 287 PNCI events were analyzed from May – August 2015, chosen to coincide with the pristine elevated initiation facet of the PECAN field campaign. A general climatology performed over a large domain, encompassing all the United States Great Plains region, from central Texas to the Canadian border. Analyses of timing of the initiation over the whole domain revealed a single major peak occurring earlier in the night while a minor peak in events occurred later in the night. Looking at all PNCI based on each subdomain, more of a dual-peaked structure became evident, suggesting some sort of non-constant forcing mechanism may be present that fluctuates during the night, thus causing the separate peaks in activity. Evolution of the LLJ over time could be considered as an explanation, however dual peak structure was observed in both plots depicting the two PNCI types that do not rely on LLJ activity, meaning LLJ evolution may not explain the overall dual-peak structure.

Elevation of each PNCI type was also analyzed, and was thought to be quite important to the actual occurrence of the initiation events. When computing relative elevations, two approaches were used, one being more general in nature than the other. The more general approach compared MLCAPE and MUCAPE values and assumed that the PNCI events were occurring at the level of the most unstable parcel, while the less general approach searched for signs of initiation at any level by examining soundings taken in the area of initiation. Each method produced quite opposite results, and since the less general, non-CAPE based approach analyzed what was going on at that location, it was thought to be more correct.

Thus, since the methods produced dissimilar results, it appears that these PNCI events are not occurring at the level of the most unstable parcel and possibly are occurring at the level with the least amount of CIN.

Analysis of both experimental high resolution models available during the PECAN field campaign as well as 16 versions of a 4km WRF-ARW model (four different PBL schemes for four PNCI cases representing each of the four types) was performed to identify trends in prediction of these initiation events and possible failure points in the models. Analysis of the PECAN models found that while overall forecasting of time initiation appeared to be fairly accurate, the more elevated and less strongly forced PNCI events tended to be predicted worse in terms of location. The WRF runs performed also revealed that elevation of the initiation may not be completely to blame for model failure. What seemed to be more important were subtle nuances in the moisture and temperature profiles that led to complete failure of the model to predict the PNCI event trying to be simulated.

Overall, forecasting nocturnal pristine convective initiation proves to be quite difficult. These initiation events lack the stronger, more obvious forcing mechanisms that aid prediction of larger scale events. Additionally, they lack the nowcasting benefits that can aid prediction of daytime surface based convection, which include monitoring via higher resolution visible satellites as well as higher density surface observations. Further research is needed to better understand the subtle and less-directly measured triggering mechanisms that accompany this hard to predict weather phenomenon.

REFERENCES

Banacos, P. C., and D. M. Schultz, 2005: The use of moisture flux convergence in forecasting convective initiation: Historical and operational perspectives. *Wea. Forecasting*, **20**, 351-366.

Bentley, M. L., and T. L. Mote, 1998: A climatology of derecho-producing mesoscale convective systems in the central and eastern United States 1986-95. Part I: Temporal and spatial distribution. *Bull. Amer. Meteor. Soc*., **79**, 2527-2540.

Bonner, W. D., 1968: Climatology of the low level jet. *Mon. Wea. Rev.*, **96**, 833-850.

_____, and J. Peagle, 1970: Diurnal variations in boundary layer winds over the south-central United States in summer. *Mon. Wea. Rev*., **98**, 735-744.

Carbone, R. E., J. D. Tuttle, D. A. Ahijevych, and S. B. Trier, 2002: Inferences of predictability associated with warm season precipitation episodes. *J. Atmos. Sci.*, **59**, 2033-2056.

Colman, B. R., 1990: Thunderstorms above frontal surfaces in environments without positive CAPE. Part I: Climatology. *Mon. Wea. Rev.*, **118**, 1103-1121.

Coniglio, M. C., J. Y. Hwang, and D. J. Stensrud, 2010: Environmental factors in the upscale growth and longevity of MCSs derived from the Rapid Update Cycle analyses. *Mon. Wea. Rev*., **138**, 3514-3539.

Doswell, C. A. III, 1987: The distinction between large-scale and mesoscale contribution to severe convection: A case study example. *Wea. Forecasting*, **2**, 3-16.

Duda, J. D., and W. A. Gallus, Jr., 2013: The impact of large-scale forcing on skill of simulated convective initiation and upscale evolution with convection-allowing grid spacings in the WRF. *Wea. Forecasting*., **28**, 994-1018.

Earth System Research Laboratory, 2016: The high-resolution rapid refresh (HRRR). Accessed 3 March 2016. [Available online at http://ruc.noaa.gov/hrrr]

Fritsch, J. M., and R. A. Maddox, 1981: Convectively driven mesoscale weather systems aloft. Part I: Observations. *J. Appl. Meteor*., **20**, 9–19.

_____, R. J. Kane, and C. R. Chelius, 1986: Contribution of mesoscale convective weather systems to the warm season precipitation in the United States. *J. Appl. Meteor*., **25**, 1333–1345.

Geerts, B. and Coauthors, 2016: The 2015 Plains Elevated Convection At Night (PECAN) field project. *Bull. Amer. Meteor. Soc.*, in press.

Hane, C. E., R. M. Rabin, T. M. Crawford, H. B. Bluestein, and M. E. Baldwin, 2002: A case study of severe storm development along a dryline within a synoptically active environment. Part II: Multiple boundaries and convective initiation. *Mon. Wea. Rev.*, **130**, 900-920.

Hong, S.-Y., S. Y. Noh, and J. Dudhia, 2006: A new vertical diffusion package with an explicit treatment of entrainment processes. *Mon. Wea. Rev.*, **134**, 2318-2341.

Jankov, I., and W. A. Gallus, 2004: MCS rainfall forecast accuracy as a function of large-scale forcing. *Wea. Forecasting*, **19**, 428–439.

Jirak, I. L., W. R. Cotton, and R.L. McAnelly, 2003: Satellite and radar survey of mesoscale convective system development. *Mon. Wea. Rev*., **131**, 2428-2449.

Keene, K. M., and R. S. Schumacher, 2013: The bow and arrow mesoscale convective structure. *Mon. Wea. Rev.*, **141**, 1648-1672.

Kingsmill, D. E., 1995: Convection initiation associated with a sea-breeze front, a gust front, and their collision. *Mon. Wea. Rev.*, **123**, 2913-2933.

Knupp, K. R., 2006: Observational analysis of a gust front to bore to solitary wave transition within an evolving nocturnal boundary layer. *J. Atmos. Sci.*, **63**, 2016-2035.

Koch, S. E., and W. L. Clark, 1999: A nonclassical cold front observed during COPS-91: Frontal structure and the process of severe storm initiation. *J. Atmos. Sci.*, **56**, 2862-2890.

Laing, A. and M. J. Fritsch, 1997: The global population of mesoscale convective complexes, *Q. R. J. Meteorol. Soc*., **123**, 389-405.

Maddox, R. A., 1980: Mesoscale convective complexes. *Bull. Amer. Meteor. Soc.*, **61**, 1374-1387.

_____, 1983: Large-scale meteorological conditions associated with midlatitude, mesoscale convective complexes. *Mon. Wea. Rev.*, **111**, 1475-1493.

_____, C. F. Chappell, and L. R. Hoxit, 1979: Synoptic and meso-α scale aspects of flash flood events. *Bull. Amer. Meteor. Soc.*, **60**, 115-123.

Mahoney, W. P. III, 1988: Gust front characteristics and the kinematics associated with interacting thunderstorm outflows. *Mon. Wea. Rev.*, **116**, 1474-1491.

Marsham, J. H., S. B. Trier, T. M. Weckwerth, and J. W. Wilson, 2011: Observations of elevated convection initiation leading to a surface-based squall line during 13 June IHOP_2002. *Mon. Wea. Rev.*, **139**, 247-271.

Mecikalski, J. R., and K. M. Bedka, 2006: Forecasting convective initiation by monitoring the evolution of moving cumulus in daytime GOES imagery. *Mon. Wea. Rev.*, **134**, 49-78.

Miller, D., and J. M. Fritsch, 1991: Mesoscale convective complexes in the western Pacific region. *Mon. Wea. Rev.*, **119**, 2978-2992.

Mitchell, M. J., R. W. Arritt, and K. Labas, 1995: A climatology of the warm season Great Plains low-level jet using wind profiler observations. *Wea. Forecasting*, **10**, 576-591.

Moncrieff, M. W., and C. Liu, 1999: Convection initiation by density currents: Role of convergence, shear, and dynamical organization. *Mon. Wea. Rev.*, **127**, 2455-2464.

Multi-scale data Assimilation and Prediction Laboratory, 2016: Realtime forecast. University of Oklahoma, Accessed 9 December 2015. [Available online at http://weather.ou.edu/~map]

Nakanishi, M., and H. Niino, 2009: Development of an improved turbulence closure model for the atmospheric boundary layer. *J. Meteor. Soc. Japan,* **87**, 895-912.

National Center for Atmospheric Research, 2016: MPAS overview. Accessed 14 March 2016. [Available online at http://mpas-dev.github.io/]

National Severe Storms Laboratory, 2016: About the NSSL realtime WRF forecasts. Accessed 10 January 2016. [Available online at http://wrf.nssl.noaa.gov/newsite/index.php?about]

Parker, M.D., 2008: Response of simulated squall lines to low-level cooling. *J. Atmos. Sci.*, **65**, 1323-1341.

Pleim, J. E., 2007: A combined local and nonlocal closure model for the atmospheric boundary layer. Part I: Model description and testing. *J. Appl. Meteor. Climatol*., **46**, 1383–1395.

Precipitation Systems Research Group, 2014: Information about CSU real-time WRF model forecasts. Colorado State University, Accessed 15 November 2015. [Available online at http://schumacher.atmos.colostate.edu/weather/csuwrf_info.php]

Reisner, J., R. M. Rasmussen, and R. Bruintjes, 1998: Explicit forecasting of supercooled liquid water in winter storms using the MM5 model. *Q. J. R. Meteorol. Soc*., **124**, 1071-1107.

Roberts, R. D., and S. A. Rutledge, 2003: Nowcasting thunderstorm initiation and growth using GOES-8 and WSR-88D data. *Wea. Forecasting*, **18**, 562-584.

Rochette, S. M., and J. T. Moore, 1996: Initiation of an elevated mesoscale convective system associated with heavy rainfall. *Wea. Forecasting*, **11**, 443-457.

Schumacher, R. S., and R. H. Johnson, 2009: Quasi-stationary, extreme-rain-producing convective systems associated with midlevel cyclonic circulations. *Wea. Forecasting*, **24**, 555-575.

Snively, D. V., and W.A. Gallus, 2014: Prediction of convective morphology in near-cloud-permitting WRF model simulations. *Wea. Forecasting*, **29**, 130-149.

Song, J., K. Liao, R. L. Coulter, and B. M. Lesht, 2005: Climatology of the low-level jet at the southern Great Plains atmospheric boundary layer experiments site. *J. App. Meteor.*, **44**, 1593-1606.

Storm Prediction Center, 2016: Mesoanalysis daily archive directory. Accessed 15 November 2015. [Available online at http://www.spc.noaa.gov/exper/ma_archive /images_s4/]

Sukoriansky, S., B. Galperin, and V. Perov, 2005: Application of a new spectral theory of stably stratified turbulence to the atmospheric boundary layer over sea ice. *Bound.-Layer Meteor.*, **117**, 231–257.

Szoke, E. J., J. Brown, and B. Shaw, 2004: Examination of the performance of several mesoscale models for convective forecasting during IHOP. Preprints, *20th Conf. on Weather Analysis and Forecasting*, Seattle, WA, Amer. Meteor. Soc., J13.6. [Available online at https://ams.confex.com/ams/pdfpapers/68930.pdf.]

Thompson, R. L., R. Edwards, J. A. Hart, K. L. Elmore, and P. M. Markowski, 2003: Close proximity sounding within supercell environments obtained from the Rapid Update Cycle. *Wea. Forecasting.*, **18**, 1243–1261.

Trier, S. B., 2003: Convective storms: convective initiation. *Encyclopedia of Atmospheric Sciences*, J. Holton, J. Pyle, and J. Curry, Ed., Elsevier, 560-570.

_____, C. A. Davis, D. A. Ahijevych, M. L. Weisman, and G. H. Bryan, 2006: Mechanisms supporting long-lived episodes of propagating nocturnal convection within a 7-day WRF model simulation. *J. Atmos. Sci.*, **63**, 2437-2461.

_____, F. Chen, and K. W. Manning, 2004: A study of convection initiation in a mesoscale model using high-resolution land surface initial conditions. *Mon. Wea. Rev.*, **132**, 2954-2976.

UCAR, 2014: Image archive, meteorological case study selection kit. Accessed 11 July 2016. [Available online at http://www2.mmm.ucar.edu/imagearchive/]

Uccellini, L. W., 1975: A case study of apparent gravity wave initiation of severe convective storms. *Mon. Wea. Rev.*, **103**, 497-513.

Velasco, I., and J. M. Fritsch, 1987: Mesoscale convective complexes in the Americas. *J. Geophys. Res.*, **92**, 9591–9613.

Wallace, J. M., 1975: Diurnal variations in precipitation and thunderstorm frequency over the conterminous United States. *Mon. Wea. Rev.*, **103**, 406–419.

Weckwerth, T. M., and R. M. Wakimoto, 1992: The initiation and organization of convective cells atop a cold-air outflow boundary. *Mon. Wea. Rev.*, **120**, 2169-2187.

Weisman, M. L., W. C. Skamarock, and J. B. Klemp, 1997: The resolution dependence of explicitly modeled convective systems. *Mon. Wea. Rev.*, **125**, 527-548.

Wilson, J. W., and R. D. Roberts, 2006: Summary of convective storm initiation and evolution during IHOP: observational and modeling perspective. *Mon. Wea. Rev.*, **134**, 23-47.

_____, and W. E. Schreiber, 1986: Initiation of convective storms at radar-observed boundary-layer convergence lines. *Mon. Wea. Rev.*, **114**, 2516-2536.

Xue, M., and W. J. Martin, 2006: A high-resolution modeling study of the 24 May 2002 dryline case during IHOP. Part II: Horizontal convective rolls and convective initiation. *Mon. Wea. Rev.*, **134**, 172-191.

Ziegler, C.L., T. J. Lee, and R. A. Pielke, Sr., 1997: Convective initiation at the dryline: A modeling study. *Mon. Wea. Rev.*, **125**, 1001-1026.

_____, and E. N. Rasmussen, 1998: The initiation of moist convection at the dryline: Forecasting issues from a case study perspective. *Wea. Forecasting*, **13**, 1106-1131.

ACKNOWLEDGEMENTS

I would like to thank my major professor, Dr. William Gallus, for his guidance throughout the entire research process, his willingness to get me involved and have hands on experience with the PECAN project, and his undying patience with me as I *slowly* finished writing my thesis. I also appreciate my other committee members, Dr. Xiaoqing Wu and Dr. Ray Arritt, for their comments and feedback. Finally, I would like to thank my family and friends, especially those graduate students and undergraduate students that both helped me technically get through the thesis process as well as kept me sane.